

Snapshot of Algebraic Vision

Joe Kileel and Kathlén Kohn

In honor of Bernd Sturmfels' 60th birthday

ABSTRACT. In this survey article, we present interactions between algebraic geometry and computer vision, which have recently come under the header of algebraic vision. The subject has given new insights in multiple view geometry and its application to 3D scene reconstruction and carried a host of novel problems and ideas back into algebraic geometry.

Computer vision is the research field that studies how computers can gain understanding from 2D images and videos, similar to human cognitive abilities. Typical computer vision tasks include the automatic recognition of objects in images, the detection of events in videos, and the reconstruction of 3D scenes from many given 2D images. A general overview of computer vision is presented in textbook form in [172]. The subject is a pillar in the AI revolution.

Algebraic vision is the symbiosis of computer vision and algebraic geometry. Motivated by Chris Aholt's Ph.D. thesis titled *Polynomials in Multiview Geometry* [9] and earlier works, the term “algebraic vision” was coined during a particular lunch held at a Seattle office of Google in early spring 2014, attended by Sameer Agarwal, Chris Aholt, Joe Kileel, Hon-Leung Lee, Max Lieblich, Bernd Sturmfels, and Rekha Thomas. The intent was to encourage interactions between the applied algebraic geometry community and the 3D reconstruction community in computer vision. A short discussion of algebraic vision can be found in the review [34] on nonlinear algebra and its applications.

Historically, computer vision made substantial use of projective geometry and computational algebra in parts of its foundations. Specifically *multiple view geometry*, as described in the textbook [94] of Hartley and Zisserman, is modeled on projective three-space and two-space and group-equivariant (multi-)linear transformations between these. Similar algebraic treatments of the subject are the textbooks [133] and [137]. Previously, this connection was not well-appreciated by the

2020 *Mathematics Subject Classification*. Primary 68T45, 14Q20, 13P25; Secondary 13P15, 65H14, 13P10.

J.K. is supported in part by NSF awards DMS-2309782 and IIS-2312746, and start-up grants from the Department of Mathematics and Oden Institute at UT Austin.

K.K. is supported in part by the Wallenberg AI, Autonomous Systems and Software Program (WASP) funded by the Knut and Alice Wallenberg Foundation.

computational algebra geometry community. However, in the last decade, algebro-geometric papers and workshops on 3D reconstruction have been appearing, leading to novel results in multiple view geometry while motivating developments in applied algebraic geometry.

The present article provides a survey of algebraic vision. No previous knowledge of computer vision is assumed, and the prerequisites for computational algebraic geometry are kept mostly to the level of undergraduate texts [51]. Due to space limitations, the article makes no attempt to be comprehensive in any way, but instead it focuses narrowly on the role of projective varieties and systems of polynomial equations in 3D vision. An outline of the sections is as follows:

- In Section 1, we introduce the problem of 3D scene reconstruction from unknown cameras and its algebro-geometric nature.
- In Section 2, we discuss a variety of usual models for cameras.
- In Section 3, we study *multiview varieties* which characterize feasible images of points under fixed cameras. Their defining equations play a key role in 3D reconstruction algorithms, and their Euclidean distance degrees measure the intrinsic complexity of noisy triangulation (i.e., the task of recovering the 3D coordinates of a point observed by known cameras).
- In Section 4, we consider the space of all cameras. We explain how tuples of cameras – up to changes of world coordinates – can be encoded via *multifocal tensors* [94].
- In Section 5, we overview the most popular algorithmic pipeline to solve 3D scene reconstruction, highlighting *minimal problems* that are the algebro-geometric heart of the pipeline.
- In Section 6, we describe polynomial solvers for minimal problems, focusing on Gröbner basis methods using *elimination templates* and homotopy continuation. Those method applies to zero-dimensional parameterized polynomial systems in general.
- In Section 7, we discuss algebro-geometric approaches to understand degenerate world scenes and image data, where uniqueness of reconstruction breaks down and algorithms can encounter difficulty.

After reading Sections 1 and 2, the other sections are essentially independent; only Section 6 builds on Section 5. We provide specific pointers to earlier sections in case of partial dependencies.

Some important topics in algebraic vision that are omitted include group synchronization (e.g., [161, 127]), uses of polynomial optimization (e.g., [104, 50, 6, 190, 44]), and approaches based on differential invariants (e.g., [42, 30]). Readers may consult [147] for a survey that covers numerical and large-scale optimization aspects in 3D reconstruction.

Acknowledgements. We thank Sameer Agarwal, Paul Breiding, Luca Carlone, Tim Duff, Hongyi Fan, Fredrik Kahl, Anton Leykin, Tomas Pajdla, Jean Ponce, Kristian Ranestad, Felix Rydell, Elima Shehu, Rekha Thomas, Matthew Trager and Uli Walther for their comments on earlier versions of the manuscript.

1. Computer vision through the algebraic lens

One of the main challenges in computer vision is the *structure-from-motion* (SfM) problem: given many 2D images, the task is to reconstruct the 3D scene

and also the positions of the cameras that took the pictures. This has many applications such as 3D mapping from images taken by drones [158], to localize and navigate autonomous cars and robots in a 3D world [83], or in the movie industry to reconstruct 3D backgrounds [107], for photo tourism [2], and for combining real and virtual worlds [60].

The structure-from-motion problem is typically solved using the 3D reconstruction pipeline. We will now sketch a highly simplified version of that pipeline, illustrated in Figure 1. We provide more details in Section 5.1. Given a set of 2D images, the first step in the pipeline is to take a few of the given images and identify geometric features, such as points or lines, that they have in common. In Figure 1b, a detection algorithm has been used that only identifies points. In the second step of the pipeline, we forget the original images and only keep the geometric features we have identified. We reconstruct the 3D coordinates of those features and also the camera poses, that is, the locations and orientations of the cameras. In Figure 1c, five common points were identified on two images, so we aim to reconstruct the five points in 3-space and the two cameras. Finally, we repeat this process several times until we have recovered all cameras and also enough geometric features to approximate the 3D scene.

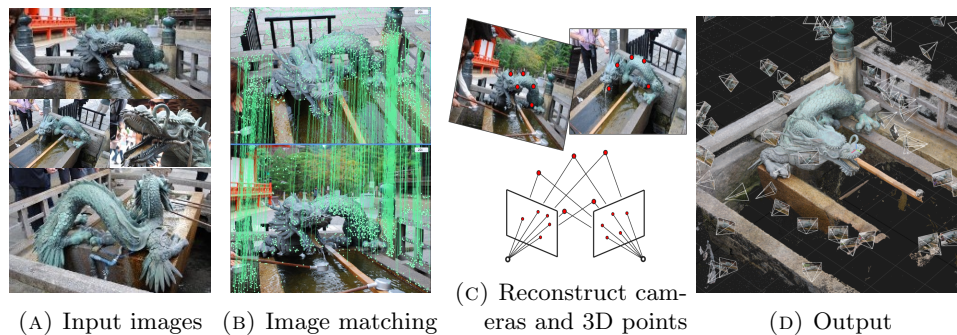


FIGURE 1. 3D reconstruction pipeline (courtesy of Tomas Pajdla).

As the second step of the pipeline forgets the pictures and only works with algebro-geometric features, such as points or lines, the reconstruction problem becomes purely algebraic. More specifically, we aim to compute a fiber of the *joint camera map*:

$$(1.1) \quad \Phi : \mathcal{X} \times \mathcal{C}_m \dashrightarrow \mathcal{Y},$$

that maps an arrangement $X \in \mathcal{X}$ of 3D features and a tuple $(C_1, \dots, C_m) \in \mathcal{C}_m$ of cameras to the m 2D images of X taken by the cameras. For instance in Figure 1c, the joint camera map becomes

$$(1.2) \quad \Phi : (\mathbb{R}^3)^5 \times \mathcal{C}_2 \dashrightarrow (\mathbb{R}^2)^5 \times (\mathbb{R}^2)^5.$$

A full specification of the joint camera map requires a choice of camera model. The simplest model is a *pinhole camera*; see Figure 2. Such a camera simply takes a picture of a point in space by projecting it onto a plane. A pinhole camera in standard position is typically assumed to be centered at the origin such that its

image plane is $H = \{(x, y, z) \in \mathbb{R}^3 \mid z = 1\}$. In these coordinates, the pinhole camera is the map

$$\mathbb{R}^3 \dashrightarrow H, \quad (x, y, z) \mapsto \left(\frac{x}{z}, \frac{y}{z}, 1\right).$$

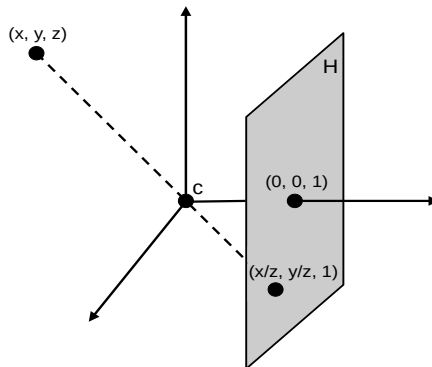


FIGURE 2. A pinhole camera in standard position is centered at $c = (0, 0, 0)$ and maps world points (x, y, z) to image points $(\frac{x}{z}, \frac{y}{z}, 1)$ on the image plane H .

Often homogeneous coordinates are used to model cameras. This means that each point in the image plane is identified with the light ray passing through the point and the origin. In homogeneous coordinates, the standard pinhole camera in Figure 2 becomes

$$\mathbb{P}_{\mathbb{R}}^3 \dashrightarrow \mathbb{P}_{\mathbb{R}}^2, \quad [x : y : z : w] \mapsto [x : y : z].$$

This map is defined everywhere except at the camera center $[0 : 0 : 0 : 1]$, i.e. the origin in the affine chart where $w = 1$.

The projective geometry approach in modeling cameras is thoroughly explained in the textbook [94]. That book laid many foundations and conventions used in modern computer vision and offers a great entry point for the algebraic community into the field of computer vision. The main focus of the book [94] is multiview geometry, where a 3D object is viewed by several cameras, such as in Figure 1. In that setting, we cannot assume that all cameras are in standard position as described above. Instead, a pinhole camera is more generally given by a 3×4 matrix A of rank three. The corresponding camera map

$$\mathbb{P}_{\mathbb{R}}^3 \dashrightarrow \mathbb{P}_{\mathbb{R}}^2, \quad X \mapsto AX.$$

is defined everywhere except at the camera center that is given by the kernel of A . The standard camera in Figure 2 corresponds to the matrix $\begin{bmatrix} 1 & 0 & 0 & 0 \\ 0 & 1 & 0 & 0 \\ 0 & 0 & 1 & 0 \end{bmatrix}$.

Hence, when using pinhole cameras and homogeneous coordinates, the *camera variety* \mathcal{C}_m in (1.1) that describes all m -tuples of such cameras is

$$\mathcal{C}_m = (\mathbb{P} \text{Mat}_3^{3 \times 4})^m,$$

where $\text{Mat}_3^{3 \times 4} \subset \mathbb{R}^{3 \times 4}$ denotes the set of 3×4 matrices of rank three. For instance, the joint camera map in (1.2) becomes

$$\begin{aligned} \Phi : (\mathbb{P}_{\mathbb{R}}^3)^5 \times (\mathbb{P} \text{Mat}_3^{3 \times 4})^2 &\dashrightarrow (\mathbb{P}_{\mathbb{R}}^2)^5 \times (\mathbb{P}_{\mathbb{R}}^2)^5, \\ (X_1, \dots, X_5, A_1, A_2) &\longmapsto (A_1 X_1, \dots, A_1 X_5, A_2 X_1, \dots, A_2 X_5). \end{aligned}$$

In the next section, we review common camera models and highlight algebraic vision articles studying camera geometry. In the remaining sections, our focus returns to the joint camera map in (1.1): We will see that many computer vision problems can be formulated using the joint camera map – such as understanding the image of a shape in space or reconstructing a 3D shape from several images – and are thus natural to study through the algebraic lens. The recent paper [1] gives a similar such unifying algebro-geometric framework for computer vision problems.

2. Camera models

Calibrated cameras. The camera model described in the previous section is known as the *projective / uncalibrated pinhole camera*. The *calibrated pinhole camera* model assumes that every camera is obtained from the standard pinhole camera in Figure 2 by translation and rotation. This means that every camera matrix A is of the form $[R \mid t]$ where $R \in \text{SO}(3)$ is the relative rotation from the standard pinhole camera to the camera with matrix A and the relative translation can be read off from the vector $t \in \mathbb{R}^3$: the camera center c , which is the origin in Figure 2, is now $c = -R^\top t$ (note that the vector $(c, 1)^\top \in \mathbb{R}^4$ spans the kernel of the camera matrix $[R \mid t]$). In particular, every calibrated pinhole camera has 6 degrees of freedom (3 for R and 3 for t), whereas a projective pinhole camera has 11 degrees of freedom.

Calibrated pinhole cameras are a commonly used model in applications, corresponding to the case when the internal parameters of the cameras are known (such as from meta data stored inside the image file). There is also a variety of *partly calibrated pinhole cameras*, e.g. a camera with unknown focal length, that have less strict structural assumptions on the 3×4 camera matrices than the fully calibrated model described above. Partly calibrated pinhole cameras are modeled as $K[R \mid t]$ where K is a 3×3 upper triangular *calibration matrix* whose entries are partially known [94, Chapter 6].

Distortion. In practice, cameras are not as ideal as in the calibrated model. As seen in Figure 2, the pinhole cameras described so far assume that the world point, the camera center, and the image point are collinear. This assumption does not hold for real-life camera lenses, because they are affected by various kinds of distortion. The main factor of deviation from the idealistic pinhole camera model is typically radial distortion; see Figure 3.

Often, calibrated cameras are a sufficient approximation of real-life cameras. However, sometimes the impact of radial distortion is too big, e.g., for fisheye cameras. One approach to address radial distortion is to make the camera model more complicated by adding distortion parameters that have to be estimated during 3D reconstruction (see [94, Chapter 7.4] for an overview and [106] for an algebraic treatment of distortion varieties). Another approach is to simplify the camera model by not estimating the radial distortion at all: Once the center of radial distortion on a given image is determined, we know for every 3D point onto which line through the distortion center it gets mapped by the camera (see Figure 3), although we

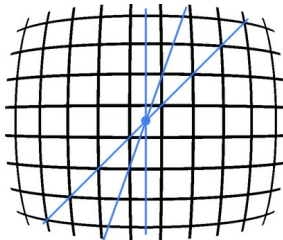


FIGURE 3. A grid affected by radial distortion. Radial lines and distortion center are blue.

do not know its exact point in the image. Thus, the camera simplifies to a map $\mathbb{P}^3 \dashrightarrow \mathbb{P}^1$ that sends 3D points to radial lines through the distortion center in the image. This is known as the *1D radial camera model* [124, 173].

Rolling shutter and pushbroom cameras. Many real-world cameras do not function like pinhole cameras that were described so far. For instance, smartphones, that produce a massive and yet growing amount of picture data, use *rolling shutters* (see e.g., [53]). When taking a picture, these cameras scan across the scene, capturing the resulting image row by row. For static cameras taking pictures of still scenes, there is no difference between rolling shutters and standard pinhole cameras that capture an entire image at the same instant (also known as global shutter). However, for moving cameras or objects, in particular videos, global shutter pinhole cameras are not a good approximation of rolling shutters. For example, when a rolling shutter camera moves with constant speed along a line, the picture of any other line in three-space would typically be a conic in the image plane, whereas a pinhole camera maps lines to lines.

A related camera model is the *pushbroom camera*, which is common in satellites [94, Chapter 6.4.1]. Such a camera considers only a plane in the 3D world that passes through the camera center and then projects that plane onto a single line. Hence, a non-moving pushbroom camera produces only an image line, not a plane. Two-dimensional images arise by moving the camera.

Rolling shutter and pushbroom cameras have received little attention from the algebraic community so far. In particular, the theory described in Sections 3–7 is largely undeveloped for such cameras.

Congruences. Ponce, Sturmfels, and Trager [154] propose a general framework to study camera geometry that includes all camera models without distortion discussed above. Their notion of a camera is an abstraction from the classical way of modeling a camera by a map $\mathbb{P}^3 \dashrightarrow \mathbb{P}^2$. Instead of identifying a concrete image plane with coordinates, they define a *rational geometric camera* to be a map $\mathbb{P}^3 \dashrightarrow \text{Gr}(1, \mathbb{P}^3)$ from three-space into the Grassmannian of lines. The fiber over any image point under a classical camera $\mathbb{P}^3 \dashrightarrow \mathbb{P}^2$ without distortion is a line, namely a *viewing ray* of the camera. The associated rational geometric camera maps each world point directly to its corresponding viewing ray. For instance, a geometric pinhole camera assigns to every world point distinct from the camera center the unique line spanned by the world point and the camera center.

The image of a rational geometric camera is a *congruence*, i.e. a two-dimensional family of lines. To obtain an actual photographic camera, one composes the geometric camera map with a map from its image congruence to \mathbb{P}^2 that models the image

formation process via mapping viewing rays to image coordinates. These physical realizations of rational geometric cameras are the focus of Trager, Sturmfels, Canny, Hebert, and Ponce in [177].

In [154], the authors suggest an even more general camera definition by saying that a *geometric camera* is an arbitrary congruence in $\text{Gr}(1, \mathbb{P}^3)$. The *order* of a congruence is the number of lines in the congruence that pass through a general point in \mathbb{P}^3 . Hence, congruences of order one are exactly those that are the images of rational geometric cameras $\mathbb{P}^3 \dashrightarrow \text{Gr}(1, \mathbb{P}^3)$. Congruences of higher order are geometric cameras such that a world point typically appears several times on each image taken by the camera. This happens for instance for many moving rolling shutter cameras, or for *catadioptric cameras* which are cameras that use curved mirrors. The idea of modeling cameras by congruences had been expressed by computer vision researchers before [149, 152, 169].

Chirality. In real life, a 3D point has to lie in front of a camera in order to be seen by it. Imposing this semialgebraic constraint on a camera model is referred to as *chirality*. The theoretical investigation of chirality was initiated by Hartley [88]; see also [94, Chapter 21]. Further studies of this concept were for instance undertaken by Laveau and Faugeras [125], Werner and Pajdla [187, 188, 185, 186], and Agarwal, Pryhuber, Sinn, and Thomas [4, 155].

3. Multiview varieties

Given m fixed pinhole cameras $C = (C_1, \dots, C_m)$, where $C_i : \mathbb{P}_{\mathbb{R}}^3 \dashrightarrow \mathbb{P}_{\mathbb{R}}^2$, we can specialize the joint camera map Φ from (1.1) to

$$(3.1) \quad \Phi_C : \mathbb{P}_{\mathbb{R}}^3 \dashrightarrow (\mathbb{P}_{\mathbb{R}}^2)^m,$$

sending a 3D point to its m images under the cameras. The *joint image* of the cameras, first introduced by Triggs [178], is $\Phi_C(\mathbb{P}_{\mathbb{R}}^3)$. The first algebraic study of the joint image was done by Heyden and Åström [96]. They called it the *natural descriptor* and observed that it is not Zariski closed. The Zariski closure $\mathcal{M}_C := \overline{\Phi_C(\mathbb{P}_{\mathbb{R}}^3)}$ of the joint image is called the *joint image variety* [175] or *multiview variety* [8]. It coincides with the Euclidean closure of the joint image [4, Theorem 4].

3.1. Multiview constraints. Many computer vision works have studied systems of polynomials that vanish on the joint image, often referred to as *multiview constraints*; see e.g. [74, 96, 73, 133, 8, 175, 5]. Their main motivation is that the joint image completely determines the cameras C_1, \dots, C_m , up to changes of coordinates in \mathbb{P}^3 . So one way of thinking about the 3D reconstruction pipeline in Figure 1 is to first obtain point correspondences between the given images (i.e., (noisy) samples on the joint image) and then estimate sufficiently many multiview constraints from the correspondences so as to be able to reconstruct the cameras, then the 3D points.

We now describe the multiview constraints studied by Heyden and Åström [96]. Let A_1, \dots, A_m be 3×4 matrices of rank three that define the cameras, i.e., $C_i : X \mapsto A_i X$. We write $x_i = (x_{i1} : x_{i2} : x_{i3})$ for the homogeneous coordinates on

the i -th image $\mathbb{P}_{\mathbb{R}}^2$, and form the $3m \times (m + 4)$ matrix

$$M_A = M_A(x_1, \dots, x_m) := \begin{bmatrix} A_1 & x_1 & 0 & \cdots & 0 \\ A_2 & 0 & x_2 & \cdots & 0 \\ \vdots & \vdots & \vdots & \ddots & \vdots \\ A_m & 0 & 0 & \cdots & x_m \end{bmatrix}.$$

A tuple of image points $(x_1, \dots, x_m) \in (\mathbb{P}_{\mathbb{R}}^2)^m$ lies in the joint image if and only if there is some 3D point X and non-zero scalars λ_i such that $A_i X = \lambda_i x_i$ for all $i = 1, \dots, m$. This implies that $[X, -\lambda_1, \dots, -\lambda_m]^\top$ is in the kernel of M_A , so the matrix M_A must be rank deficient. In fact, the multiview variety \mathcal{M}_C is cut out by the maximal minors of M_A :

$$(3.2) \quad \mathcal{M}_C = \{(x_1, \dots, x_m) \in (\mathbb{P}_{\mathbb{R}}^2)^m \mid \text{rk } M_A(x_1, \dots, x_m) < m + 4\}.$$

These maximal minors are multilinear, i.e. they are linear in every triplet x_i of variables.

EXAMPLE 3.1. For $m = 2$ cameras, M_A is a 6×6 matrix. Its determinant defines the multiview hypersurface \mathcal{M}_C in $\mathbb{P}_{\mathbb{R}}^2 \times \mathbb{P}_{\mathbb{R}}^2$. This equation is a bilinear form in x_1, x_2 represented by a matrix $F \in \mathbb{R}^{3 \times 3}$, i.e. $\det(M_A) = x_2^\top F x_1$. Here F is called the *fundamental matrix* for projective pinhole cameras, and the *essential matrix* for calibrated pinhole cameras. Longuet-Higgins' seminal work [131] introduced the essential matrix to the computer vision community along with a first 3D reconstruction algorithm. We will discuss essential matrices, fundamental matrices, and their generalizations to more than two cameras in Section 4.

For every subset $J \subseteq \{1, \dots, m\}$ of cardinality k , we consider the $3k \times (k + 4)$ submatrix $M_{A,J}$ of M_A whose rows and columns correspond to the cameras C_j for $j \in J$. As the maximal minors of $M_{A,J}$ are multilinear constraints in the k triplets of variables $\{x_j \mid j \in J\}$, we refer to the set of all maximal minors of all $M_{A,J}$ with $|J| = k$ as the k -linearities. As seen in (3.2), the multiview variety \mathcal{M}_C of m cameras is cut out by the m -linearities. Heyden and Åström [96] showed that \mathcal{M}_C is in fact cut out by the 2-linearities if the m camera centers are not coplanar.

An ideal-theoretic treatment of the multiview variety was first done by Aholt, Sturmfels, and Thomas [8], and later continued by Agarwal, Pryhuber, and Thomas [5]. They study the vanishing ideal of \mathcal{M}_C , called the *multiview ideal*.

- THEOREM 3.2. (1) *If the m camera centers are pairwise distinct, the multiview ideal is generated by the 2- and 3-linearities [5, Theorem 3.7].*
 (2) *If all 4×4 minors of the $4 \times 3m$ matrix $[A_1^\top \ A_2^\top \ \cdots \ A_m^\top]$ are non-zero, then the 2-, 3-, and 4-linearities form a universal Gröbner basis of the multiview ideal [8, Theorem 2.1].*

A nice overview of the joint image and its Zariski closure (equivalently, Euclidean closure) is presented in *the joint image handbook* by Trager, Hebert, and Ponce [175]. They provide an explicit description of the actual joint image (instead of its closure) as a constructible set, and discuss sets of k -linearities that cut out the multiview variety as well as sets of k -linearities that are not sufficient to define \mathcal{M}_C but uniquely determine the cameras C_1, \dots, C_m , up to coordinates changes in $\mathbb{P}_{\mathbb{R}}^3$.

3.2. Euclidean distance degree and triangulation. *Triangulation* refers to the problem of reconstructing the 3D coordinates of a point from 2D images when the cameras are known. For pinhole cameras $C = (C_1, \dots, C_m)$, this means to compute the fiber of the specialized joint camera map Φ_C in (3.1). In theory, triangulation is trivial to solve for $m \geq 2$ cameras, since the fiber under each camera $C_i : \mathbb{P}_{\mathbb{R}}^3 \dashrightarrow \mathbb{P}_{\mathbb{R}}^2$ is a line and so the desired 3D point is the intersection of these m lines in $\mathbb{P}_{\mathbb{R}}^3$. However, in practice, the image measurements are noisy, which means that the given image points $(x_1, \dots, x_m) \in (\mathbb{P}_{\mathbb{R}}^2)^m$ do not lie on the multiview variety \mathcal{M}_C . Thus, to solve triangulation, one first needs to *denoise* the given data, for instance by finding a nearby point on the multiview variety \mathcal{M}_C to the given data point $x = (x_1, \dots, x_m) \in (\mathbb{P}_{\mathbb{R}}^2)^m$.

In practical applications, the given image points are finite, which means that after a choice of affine chart \mathbb{R}^2 of each $\mathbb{P}_{\mathbb{R}}^2$ we may assume that $x \in \mathbb{R}^{2m}$. In this setting, we want to find the closest point x on the restriction of \mathcal{M}_C to the chosen affine chart, that is, on the *affine multiview variety*:

$$\mathcal{M}_C^\alpha = \mathcal{M}_C \cap \mathbb{R}^{2m}.$$

Typically, distance is measured via the squared Euclidean distance on \mathbb{R}^{2m} . Regarding \mathcal{M}_C^α as a complex variety in \mathbb{C}^{2m} , for almost all data points $x \in \mathbb{C}^{2m}$, this optimization problem has a constant number of complex critical points [61]. That number is known as the *Euclidean distance degree* (*ED degree* for short) of the variety \mathcal{M}_C^α . ED degree measures the algebraic complexity of the triangulation problem, in the sense that it provides an upper bound for the number of real critical points for generic data points $x \in \mathbb{R}^{2m}$.

Hartley and Sturm [92] showed that the ED degree of the affine multiview variety $\mathcal{M}_{(C_1, C_2)}^\alpha$ for two cameras is 6. Stewénus and Nistér computed the ED degree of \mathcal{M}_C^α for $m \leq 7$ cameras and observed that it grows cubically [90]. The problem of determining the ED degree of the affine multiview variety actually motivated the general introduction of Euclidean distance degrees of algebraic varieties by Draisma, Horobet, Ottaviani, Sturmfels, and Thomas [61, Example 3.3], as well as follow-up work on orthogonally invariant matrix sets [63, 62]. In [61, Conjecture 3.4], a precise cubic formula for the ED degree of \mathcal{M}_C^α for an arbitrary number of cameras was conjectured. Harris and Lowengrub [86] provided an upper bound for the ED degree, showing that it is indeed bounded by some cubic polynomial in the number of cameras, before [61, Conjecture 3.4] was finally proven by Maxim, Rodriguez, and Wang:

THEOREM 3.3 ([136]). *When the $m \geq 2$ cameras are in general position, the Euclidean distance degree of the affine multiview variety \mathcal{M}_C^α is*

$$\frac{9}{2}m^3 - \frac{21}{2}m^2 + 8m - 4.$$

Informally, the theorem means triangulation with a large number of cameras may be quite difficult: the number of critical points grows cubically with m .

3.3. Extensions. There are several extensions of multiview varieties which incorporate additional constraints or apply to different models. We discuss some recent extensions below.

Chirality. The discussion of multiview varieties and triangulation above ignores the constraint of chirality, i.e., that the 3D point must lie in front of each

camera in order to be seen by it. Agarwal, Pryhuber, Sinn, and Thomas [4] provide semialgebraic descriptions (using polynomial equalities and inequalities) of both the *chiral domain*, that is the set of points in $\mathbb{P}_{\mathbb{R}}^3$ that lie in front of each of the m pinhole cameras C_i , and the *chiral joint image*, i.e. the image of the chiral domain under the specialized joint camera map Φ_C in (3.1). The chiral joint image is a subset of Triggs' joint image $\Phi_C(\mathbb{P}_{\mathbb{R}}^3)$ [178] and describes the true image of the 3D world as seen by the cameras $C = (C_1, \dots, C_m)$. Hence, the semialgebraic description of the chiral joint image from [4] is a refinement of the multiview constraints discussed above.

Congruences. Multiview varieties can be naturally generalized to other camera models (besides pinhole cameras as described above). Recall that a rational geometric camera is a map

$$\mathbb{P}^3 \dashrightarrow \Sigma \subset \text{Gr}(1, \mathbb{P}^3)$$

that maps a world point X to a line passing through X . The Zariski closure of the image of the map is a congruence Σ , i.e. a surface in the Grassmannian $\text{Gr}(1, \mathbb{P}^3)$ of lines. The map is defined everywhere except at its *focal locus*, that is, the set of points $X \in \mathbb{P}^3$ that belong to more than one line on Σ .

Given m rational geometric cameras $C = (C_1, \dots, C_m)$, $C_i : \mathbb{P}^3 \dashrightarrow \Sigma_i \subset \text{Gr}(1, \mathbb{P}^3)$, the *multi-image variety* \mathcal{M}_C is the Zariski closure of the image of

$$\Phi_C : \mathbb{P}^3 \dashrightarrow \Sigma_1 \times \dots \times \Sigma_m \subset \text{Gr}(1, \mathbb{P}^3)^m, \quad X \mapsto (C_1(X), \dots, C_m(X)).$$

Ponce, Sturmfels, and Trager [154] showed that the multi-image variety often has an easy description in terms of the *concurrent lines variety* $V_m \subset \text{Gr}(1, \mathbb{P}^3)^m$ that consists of all m -tuples of lines that meet in a common point.

THEOREM 3.4 ([154, Theorem 5.1]). *If the m focal loci of the cameras C_1, \dots, C_m are pairwise disjoint, then $\mathcal{M}_C = V_m \cap (\Sigma_1 \times \dots \times \Sigma_m)$.*

The authors also describe a minimal set of generators and a reduced Gröbner bases for the prime ideal of the concurrent lines variety V_m in [154, Theorem 3.1]. Moreover, using the Plücker embedding $\text{Gr}(1, \mathbb{P}^3) \subset \mathbb{P}^5$, they conjectured a formula for the multidegree of V_m in $(\mathbb{P}^5)^m$, which was proven by Escobar and Knutson [68, Theorem 2.4]. The latter theorem also provides the multidegree of the multi-image variety \mathcal{M}_C in $(\mathbb{P}^5)^m$ under the assumption that the m focal loci of the cameras C_1, \dots, C_m are pairwise disjoint.

3D data. Another way to generalize multiview varieties is by not only considering the image of a single 3D point under the given cameras, but rather instead considering the image of more complex 3D objects. The *line multiview variety*, i.e., the Zariski closure of the image of the map $\text{Gr}(1, \mathbb{P}^3) \dashrightarrow (\text{Gr}(1, \mathbb{P}^2))^m$ that sends a 3D line to its images under m pinhole cameras, is described in [35, 74]. Multiview varieties for more than one point are studied in [102]. For instance, the authors there consider the set of point pairs in $\mathbb{R}^3 \times \mathbb{R}^3$ that are a Euclidean distance of 1 apart from each other. Let $\mathcal{X} \subset \mathbb{P}_{\mathbb{R}}^3 \times \mathbb{P}_{\mathbb{R}}^3$ be the Zariski closure of said set. Given m pinhole cameras $C = (C_1, \dots, C_m)$, the authors restrict the joint camera map from (1.1) to:

$$(3.3) \quad \mathcal{X} \dashrightarrow (\mathbb{P}_{\mathbb{R}}^2)^m \times (\mathbb{P}_{\mathbb{R}}^2)^m, \quad (X_1, X_2) \mapsto (\Phi_C(X_1), \Phi_C(X_2)),$$

and define the *rigid multiview variety* as the Zariski closure of the image of this map. They derive a set of polynomial equations cutting out the rigid multiview

variety and give a conjecture for a minimal generating set of its prime ideal. The authors of [102] also describe defining polynomial equations for other variations of multiview varieties, e.g. when \mathcal{X} in (3.3) is instead taken to be an arbitrary hypersurface in $\mathbb{P}_{\mathbb{R}}^3 \times \mathbb{P}_{\mathbb{R}}^3$, or when \mathcal{X} is in $(\mathbb{P}_{\mathbb{R}}^3)^3$ and consists of triples of points with fixed pairwise Euclidean distances, or when \mathcal{X} is in $(\mathbb{P}_{\mathbb{R}}^3)^4$ and consists of all 4-tuples of points that lie on a common plane in $\mathbb{P}_{\mathbb{R}}^3$.

Higher dimensions. Several works have studied higher-dimensional generalizations of the specialized joint camera map in (3.1), i.e., maps from a projective space onto a product of projective spaces, all of arbitrary dimension, e.g. [128, 100, 49]. The study of higher-dimensional pinhole cameras is motivated by capturing *dynamic scenes*. We will sketch this application and some higher-dimensional extensions of multiview varieties in Section 4.3.5.

4. Understanding camera tuples

4.1. Symmetry of joint camera map. The joint camera map $\Phi : \mathcal{X} \times \mathcal{C}_m \dashrightarrow \mathcal{Y}$ often carries a symmetry: depending on the specific camera models and 3D object types, there exists a group G acting on the fibers of Φ . This symmetry arises by simultaneously acting on the cameras and the 3D objects via 3D change of coordinates which preserve the camera model and 3D objects. This has the important implication that in 3D reconstruction (such as structure-from-motion) we cannot hope to precisely recover a world scene $(X, (C_1, \dots, C_m))$ from its 2D image data $\Phi(X, (C_1, \dots, C_m))$. Instead the best we can reconstruct is the world scene up the action of G .

For example, if $\mathcal{C}_m = (\mathbb{P}\text{Mat}_3^{3 \times 4})^m$ consists of tuples of projective pinhole cameras and $\mathcal{X} = (\mathbb{P}_{\mathbb{R}}^3)^n$ consists of tuples of points in 3D projective space, then the group G is the projective general linear group $G = \text{PGL}(4, \mathbb{R})$. Indeed, note

$$Ax = (Ag)(g^{-1}x)$$

for each $A \in \text{Mat}_3^{3 \times 4}$, $x \in \mathbb{P}^3$ and $g \in \text{PGL}(4, \mathbb{R})$. In this case, we can only aim to recover the world scene up to a projective transformation.

As another example, suppose that \mathcal{C}_m consists of tuples of calibrated cameras $([R_1|t_1], \dots, [R_m|t_m])$ where $R_i \in \text{SO}(3)$ and $t_i \in \mathbb{R}^3$. Take $\mathcal{X} = (\mathbb{P}^3)^n$ again to consist of tuples of 3D projective points. Now the relevant group is

$$(4.1) \quad G = \left\{ g \in \text{GL}(4, \mathbb{R}) : g = \begin{bmatrix} R & t \\ 0 & \lambda \end{bmatrix} \text{ for some } R \in \text{SO}(3), t \in \mathbb{R}^3, \lambda \in \mathbb{R} \setminus \{0\} \right\},$$

i.e., the scaled special Euclidean group of \mathbb{R}^3 (also known as the similarity group). This is because G is the largest subgroup of 3D changes of coordinates which maps calibrated cameras to calibrated cameras. the world scene is ambiguous up to a proper rigid motion R , and a central scale λ , t So when we know the cameras are calibrated, the world scene is ambiguous up to a proper rigid motion (R, t) and a central scale (λ) .

A novel approach to detect all symmetries in a given 3D reconstruction problem has been recently developed by Duff, Korotynskiy, Pajdla, and Regan [66]. Their approach is based on based on *Galois / monodromy groups*, and uses numerical homotopy continuation computations (cf. Section 6.2 below).

4.2. Camera configurations. To cope with such ambiguities, it has been useful in computer vision to consider *camera tuples modulo the relevant symmetries*. Working out camera tuples modulo symmetries can be viewed as one of the accomplishments of multiview geometry [94]. From a mathematical standpoint, Aholt and Oeding observed in [7] that formally we can regard the space of possible camera configurations as the GIT quotient:

$$(4.2) \quad \mathcal{C}_m // G.$$

Here GIT stands for geometric invariant theory, developed by Mumford [141]. The GIT quotient $\mathcal{C}_m // G$ is an abstract, non-embedded scheme or stack. While this GIT description can be made precise to the abstract algebraic geometer, it would not be useable in 3D reconstruction problems. The perspective does tell us that multiview geometry found certain explicit birational models for these GIT quotients, which are useful for 3D reconstruction.

4.3. Multifocal tensors. Camera configurations are represented by *multifocal tensors* in multiview geometry. We present them for configurations of two, three and four cameras, and then give a higher-dimensional construction called *Grassmann tensors* [91] motivated by dynamic scenes.

4.3.1. Two projective cameras: fundamental matrices. Fix two projective pinhole cameras $C_1, C_2 : \mathbb{P}^3 \dashrightarrow \mathbb{P}^2$ represented by matrices A_1, A_2 . Consider the set of corresponding point pairs defined as the multiview variety:

$$\mathcal{M}_C = \{(x_1, x_2) \in \mathbb{P}^2 \times \mathbb{P}^2 : \exists X \in \mathbb{P}^3 \text{ s.t. } C_1(X) = x_1, C_2(X) = x_2\}.$$

This set is invariant under the action of $G = \text{PGL}(4, \mathbb{R})$ on $C = (C_1, C_2)$, i.e. it depends only on the configuration C modulo G . On the other hand, \mathcal{M}_C is generically a hypersurface of bidegree $(1, 1)$ as explained in Example 3.1:

$$\begin{aligned} \mathcal{M}_C &= \left\{ (x_1, x_2) : \exists X \in \mathbb{P}^3 \exists \lambda_1, \lambda_2 \in \mathbb{R} \text{ s.t. } \begin{bmatrix} A_1 & x_1 & 0 \\ A_2 & 0 & x_2 \end{bmatrix} \begin{bmatrix} X \\ -\lambda_1 \\ -\lambda_2 \end{bmatrix} = 0 \right\} \\ &= \left\{ (x_1, x_2) : \det \begin{bmatrix} A_1 & x_1 & 0 \\ A_2 & 0 & x_2 \end{bmatrix} = 0 \right\}. \end{aligned}$$

This equation for \mathcal{M}_C may be written as $x_2^\top F x_1 = 0$ where for $1 \leq i, j \leq 3$,

$$F_{ij} = (-1)^{i+j} \det \begin{bmatrix} A_{1,\hat{j}} \\ A_{2,\hat{i}} \end{bmatrix},$$

where $A_{1,\hat{j}}$ denotes A_1 with the j th row dropped and likewise for $A_{2,\hat{i}}$. One regards F as in $\mathbb{P}(\text{Mat}^{3 \times 3})$, that is, defined only up to nonzero scale. In multiview geometry, F is called the *fundamental matrix* for the pair of cameras C . It may be shown that F generically determines C modulo G [94], thus F furnishes an explicit model for the configuration. The collection of all F arising in this way is exactly the set of rank 2 matrices, $\mathbb{P}(\text{Mat}_2^{3 \times 3})$, with Zariski closure given by the determinantal variety $\{F \in \mathbb{P}(\text{Mat}^{3 \times 3}) : \det(F) = 0\}$. The construction is practically useful in 3D reconstruction because point pairs in \mathcal{M}_C can be detected in real-life 2D images.

4.3.2. Two calibrated cameras: Essential matrices. We can restrict the fundamental matrix construction to the case of two calibrated cameras. The restriction yields a subset of the fundamental matrices, whose points are called *essential matrices* and customarily denoted by E in computer vision. Demazure [57] determined that the resulting subvariety of the determinantal variety is 5 dimensional, degree 10, with ideal minimally generated by the following ten cubic equations:

$$(4.3) \quad \det(E) = 0 \quad \text{and} \quad EE^\top E - \frac{1}{2} \text{trace}(EE^\top)E = 0.$$

Another description is that essential matrices $E \in \mathbb{P}(\text{Mat}^{3 \times 3})$ are those with rank 2 whose top singular values are equal, i.e. $\sigma_1(E) = \sigma_2(E) > \sigma_3(E) = 0$. Yet another description is that, after taking the *complex* Zariski closure, the variety of essential matrices can be realized as a complex hyperplane section of the determinantal variety of rank ≤ 2 symmetric 4×4 matrices [77].

Here E only depends on C modulo the relevant group, i.e. the scaled special Euclidean group G (4.1). In this case however, the association of a calibrated configuration to an essential matrix is generically two-to-one (cf. *twisted pairs* in [94]). Thus the GIT quotient (4.2) gives a degree-2 cover of the variety of essential matrices. The advantage of essential matrices is that they capture corresponding image point pairs which can be detected in real-life images.

4.3.3. Three cameras: Trifocal tensors. Given three projective cameras $C_1, C_2, C_3 : \mathbb{P}^3 \dashrightarrow \mathbb{P}^2$ represented by matrices A_1, A_2, A_3 , consider the set of corresponding point-line-line triples:

$$\Psi_C = \left\{ (x_1, \ell_2, \ell_3) \in \mathbb{P}^2 \times (\mathbb{P}^2)^* \times (\mathbb{P}^2)^* : \right. \\ \left. \exists X \in \mathbb{P}^3 \text{ s.t. } C_1(X) = x_1, C_2(X) \in \ell_2, C_3(X) \in \ell_3 \right\},$$

where $(\mathbb{P}^2)^*$ is the dual projective plane consisting of lines in \mathbb{P}^2 . It then holds

$$\Psi_C = \left\{ (x_1, \ell_2, \ell_3) : \exists X \in \mathbb{P}^3 \exists \lambda_1 \in \mathbb{R} \text{ s.t. } \begin{bmatrix} A_1 & x_1 \\ \ell_2^\top A_2 & 0 \\ \ell_3^\top A_3 & 0 \end{bmatrix} \begin{bmatrix} X \\ -\lambda_1 \end{bmatrix} = 0 \right\} \\ = \left\{ (x_1, \ell_2, \ell_3) : \det \begin{bmatrix} A_1 & x_1 \\ \ell_2^\top A_2 & 0 \\ \ell_3^\top A_3 & 0 \end{bmatrix} = 0 \right\},$$

where we have identified ℓ_i with its normal vector of 3 homogeneous coordinates. The equation for Ψ_C may be written using tensor contraction as $T(x_1, \ell_2, \ell_3) = 0$ where $T \in \mathbb{P}(\mathbb{R}^{3 \times 3 \times 3})$ is given by

$$T_{ijk} = (-1)^{i+j+k} \det \begin{bmatrix} A_{1,i} \\ A_{2,j} \\ A_{3,\hat{k}} \end{bmatrix}$$

for $1 \leq i, j, k \leq 3$. Here $A_{1,i}$ denotes the i th row of A_1 , likewise for $A_{2,j}$, and $A_{3,\hat{k}}$ denotes A_3 with the k th row removed. In multiview geometry T is known as the *trifocal tensor* associated with the camera triple C . The map from (C_1, C_2, C_3) modulo $\text{PGL}(4, \mathbb{R})$ to T is generically one-to-one, so the Zariski closure of the set of trifocal tensors is a birational model for configurations of three (projective) cameras. As proven in [7], the trifocal tensors variety has dimension 18, degree 297 and an ideal minimally generated by 10 polynomials in degree 3, 81 polynomials

in degree 5, and 1980 polynomials in degree 6. Trifocal tensors are relevant to 3D reconstruction, because of their relation to image correspondence data. They capture point-line-line correspondences by definition via tensor-vector contraction. However it is also true that trifocal tensors capture other correspondence types (e.g., point-point-point) via other multilinear algebraic operations, see [94, Part III] for details.

If we restrict (C_1, C_2, C_3) to calibrated pinhole cameras, then we obtain only certain trifocal tensors and a subvariety called the *calibrated trifocal variety* in [105]. The calibrated trifocal variety is a birational model for the GIT quotient of triples of calibrated cameras modulo the scaled special Euclidean group G (4.1). Currently the ideal defining the variety is partially understood [135].

4.3.4. Four cameras: Quadrifocal tensors. A similar construction can be carried out for four projective pinhole cameras C_1, C_2, C_3, C_4 based on correspondences between quadruples of image lines:

$$\begin{aligned} & \{(\ell_1, \ell_2, \ell_3, \ell_4) \in (\mathbb{P}^2)^* \times (\mathbb{P}^2)^* \times (\mathbb{P}^2)^* \times (\mathbb{P}^2)^* : \\ & \quad \exists X \in \mathbb{P}^3 \text{ s.t. } C_1(X) \in \ell_1, C_2(X) \in \ell_2, C_3(X) \in \ell_3, C_4(X) \in \ell_4\}. \end{aligned}$$

Similarly to the above, this is a hypersurface defined by $Q(\ell_1, \ell_2, \ell_3, \ell_4) = 0$ where $Q \in \mathbb{P}(\mathbb{R}^{3 \times 3 \times 3 \times 3})$ is given by

$$Q_{ijkl} = (-1)^{i+j+k+l} \det \begin{bmatrix} A_{1,i} \\ A_{2,j} \\ A_{3,k} \\ A_{4,l} \end{bmatrix}$$

The tensor Q is known as the *quadrifocal tensor* in multiple view geometry. The ideal of the Zariski closure of quadrifocal tensors was studied up to degree 9 in [145]. Quadrifocal tensors for calibrated cameras have not been investigated.

4.3.5. Dynamic scenes. The fundamental matrix and the trifocal and quadrifocal tensors (and their calibrated counterparts) are used for the reconstruction of static scenes. There are many approaches for the reconstruction of dynamic scenes, i.e., where the 3D points undergo different motions. Here we highlight two algebraic ideas.

Wolf and Shashua [189] and Huang, Fossum and Ma [99] argue that many motions of 3D points can be modeled by embedding them into a larger dimensional space such that the camera map becomes a projection of the form $\mathbb{P}^N \dashrightarrow \mathbb{P}^2$. This motivated Hartley and Schaffalitzky [91] to construct the Grassmann tensor, which we explain in Section 4.3.6 below. For instance, a 3D point $X = (X_1, X_2, X_3, 1)^\top$ that moves linearly in an affine chart of \mathbb{P}^3 with constant velocity in the direction $V = (V_1, V_2, V_3, 0)^\top$ can be embedded into \mathbb{P}^6 as follows: $\bar{X} = (V_1 : V_2 : V_3 : X_1 : X_2 : X_3 : 1)^\top$. If A_i denotes the 3×4 matrix representing a moving pinhole camera at time i , the image taken of the moving point X at time i is $A_i(X + iV)$. Writing A'_i for the left-most 3×3 submatrix of A_i and $\bar{A}_i = [iA'_i \mid A_i] \in \mathbb{R}^{3 \times 7}$, we can express the image as $A_i(X + iV) = \bar{A}_i \bar{X}$. Hence, the camera map is a projection $\mathbb{P}^6 \dashrightarrow \mathbb{P}^2$.

Another algebraic approach to dynamic scenes was suggested by Vidal and coauthors [184, 72]. Suppose that a scene observed by a pinhole camera has n independently moving objects and that we take two pictures of the scene at two different times. For each of the n objects, we have a fundamental matrix F_i

describing the relative pose of the object at the two instants of time. Any pair of image points (x_1, x_2) coming from a common 3D point must lie on one of the n objects and thus satisfies the equation $(x_2^\top F_1 x_1) \cdots (x_2^\top F_n x_1) = 0$. As this equation is homogeneous of degree n in both x_1 and x_2 , we can apply the Veronese embedding $\nu_n : \mathbb{P}^2 \rightarrow \mathbb{P}^N$, $N = \binom{n+2}{2} - 1$, to obtain the following bilinear equation in $\nu(x_1)$ and $\nu(x_2)$: $\nu(x_2)^\top F \nu(x_1) = 0$, where $F \in \mathbb{R}^{N \times N}$ is called the *multibody fundamental matrix*. This construction has been generalized, e.g. to *multibody trifocal tensors* [93] and other motion models [182]. Finally, we note that 3D motion segmentation from m views, i.e., the problem to determine the number n of moving objects and which given m -tuples of image points belong to which object, can also be solved with *generalized principal component analysis (GPCA)*. GPCA is a method considered by Vidal, Ma, and Sastry to fit an unknown number of linear subspaces of unknown dimensions to given data points in a real vector space [183]. Other algebraic methods for GPCA include [180].

4.3.6. Grassmann tensors. Here we review the Grassmann tensor construction of Hartley and Schaffalitzky [91] that unifies multifocal tensors with higher-dimensional generalizations. Consider \mathbb{P}^N , noting that $N > 3$ can model dynamic scenes as in Section 4.3.5. Let $C_i : \mathbb{P}^N \dashrightarrow \mathbb{P}^{n_i}$, $X \mapsto A_i X$ be m surjective linear projections. Assume $m \leq N + 1 \leq \sum_{i=1}^m n_i$. Then we can fix integers c_1, \dots, c_m satisfying $1 \leq c_i \leq n_i$ and $c_1 + \dots + c_m = N + 1$. The special cases $n_i = 2$ and $n_i = 1$ appear in pinhole cameras and 1D radial cameras [124, 173], respectively.

Write $\text{Gr}(n - c, \mathbb{P}^n)$ for the Grassmannian of linear subspaces of \mathbb{P}^n of codimension c . The main object is the set of “corresponding subspace tuples”:

$$(4.4) \quad \{(L_1, \dots, L_m) \in \text{Gr}(n_1 - c_1, \mathbb{P}^{n_1}) \times \dots \times \text{Gr}(n_m - c_m, \mathbb{P}^{n_m}) : \\ \exists X \in \mathbb{P}^N \text{ s.t. } C_1(X) \in L_1, \dots, C_m(X) \in L_m\}.$$

The authors of [91] proved that (4.4) is an algebraic hypersurface; moreover its defining equation is multilinear in the Plücker coordinates for the Grassmannians. Thus, the coefficients of defining equation form an m -way tensor

$$\mathbf{T} = \mathbf{T}_{(C_1, \dots, C_m), (c_1, \dots, c_m)}$$

of size $\binom{n_1+1}{c_1} \times \dots \times \binom{n_m+1}{c_m}$. One calls \mathbf{T} the *Grassmann tensor* for the projections (C_1, \dots, C_m) with respect to the codimensions (c_1, \dots, c_m) [91]. The authors proved that \mathbf{T} depends only on (C_1, \dots, C_m) modulo $\text{PGL}(N + 1, \mathbb{R})$. Further, if at least n_i strictly exceeds 1 then (C_1, \dots, C_m) modulo $\text{PGL}(N + 1)$ is generically uniquely determined by \mathbf{T} . Fundamental matrices, trifocal tensors and quadrifocal tensors correspond to $N = 3$ and $(c_1, c_2) = (2, 2)$, $(c_1, c_2, c_3) = (2, 1, 1)$ and $(c_1, c_2, c_3, c_4) = (1, 1, 1, 1)$ respectively.

The construction of \mathbf{T} can be derived here. For $L_i \in \text{Gr}(n_i - c_i, \mathbb{P}^{n_i})$ we choose a basis of the dual space $L_i^* \subseteq (\mathbb{P}^{n_i})^*$ comprised of the hyperplanes containing L_i ; let the basis be

$$\mathcal{V}_i = \{v_{i1}, \dots, v_{ic_i}\} \subseteq (\mathbb{P}^{n_i})^*.$$

The dual linear map $C_i^* : (\mathbb{P}^{n_i})^* \rightarrow (\mathbb{P}^N)^*$ pulls \mathcal{V}_i back to $(\mathbb{P}^N)^*$ to give

$$A_i^\top \mathcal{V}_i = \{A_i^\top v_{i1}, \dots, A_i^\top v_{ic_i}\} \subseteq (\mathbb{P}^N)^*.$$

The requirement on $X \in \mathbb{P}^N$ in (4.4) is $\langle A_i X, v_{ij} \rangle = 0$ for each i, j , or equivalently $\langle X, A_i^\top v_{ij} \rangle = 0$. Hence we require $A_1^\top \mathcal{V}_1 \cup \dots \cup A_m^\top \mathcal{V}_m$ to not span $(\mathbb{P}^N)^*$, i.e.

$$(4.5) \quad [A_1^\top v_{11} \quad \dots \quad A_1^\top v_{1c_1} \quad \dots \quad \dots \quad A_m^\top v_{m1} \quad \dots \quad A_m^\top v_{mc_m}] \in \mathbb{R}^{(N+1) \times (N+1)}.$$

is rank-deficient. The matrix (4.5) factors as

$$(4.6) \quad \underbrace{\begin{bmatrix} A_1^\top & A_2^\top & \dots & A_m^\top \end{bmatrix}}_{=A^\top} \underbrace{\begin{bmatrix} \mathcal{V}_1 & 0 & \dots & 0 \\ 0 & \mathcal{V}_2 & \dots & 0 \\ \vdots & \vdots & \ddots & \vdots \\ 0 & 0 & \dots & \mathcal{V}_m \end{bmatrix}}_{=\mathcal{V}}.$$

We require the determinant of (4.6) to vanish, which by the Cauchy-Binet formula is

$$(4.7) \quad \sum_{\substack{\mathcal{I} \subseteq [(n_1+1)+\dots+(n_m+1)] \\ \#\mathcal{I}=N+1}} \det(A^\top[:, \mathcal{I}]) \det(\mathcal{V}[\mathcal{I}, :]).$$

Here $A^\top[:, \mathcal{I}]$ denotes the $(N+1) \times (N+1)$ submatrix consisting of the columns indexed by \mathcal{I} , etc. Recalling that the rows in \mathcal{V} containing $\mathcal{V}_i \in \mathbb{R}^{(n_i+1) \times c_i}$ have rank c_i and that $c_1 + \dots + c_m = N+1$, we can restrict the sum in (4.7) as follows:

$$\sum_{\substack{\mathcal{I}_1 \subseteq [n_1+1] \\ \#\mathcal{I}_1=c_1}} \dots \sum_{\substack{\mathcal{I}_m \subseteq [n_m+1] \\ \#\mathcal{I}_m=c_m}} \det(A_1^\top[:, \mathcal{I}_1] \dots A_m^\top[:, \mathcal{I}_m]) \prod_{i=1}^m \det(\mathcal{V}_i[\mathcal{I}_i, :]).$$

At this point, note $\det(\mathcal{V}_i[\mathcal{I}_i, :])$ for $\mathcal{I}_i \subseteq [n_i+1]$ are the dual Plücker coordinates of $L_i \in \text{Gr}(n_i - c_i, \mathbb{P}^{n_i})$. These depend on the choice of basis \mathcal{V}_i only through a global nonzero scale, and (after sign flips) equal the primal Plücker coordinates of L_i up to scale. That is, letting $\mathcal{U}_i = \{u_{i1}, \dots, u_{i, n_i - c_i + 1}\} \subseteq \mathbb{P}^{n_i}$ be a basis for L_i one has

$$(4.8) \quad \left(\det(\mathcal{V}_i[\mathcal{I}_i, :]) \mid \mathcal{I}_i \subseteq [n_i+1], \#\mathcal{I}_i = c_i \right) \\ \propto \left((-1)^{c_i + \sum \mathcal{I}_i} \det(\mathcal{U}_i[\mathcal{I}_i^c, :]) \mid \mathcal{I}_i \subseteq [n_i+1], \#\mathcal{I}_i = c_i \right),$$

where $\mathcal{I}_i^c = [n_i+1] \setminus \mathcal{I}_i$ and $\sum \mathcal{I}_i = \sum_{\ell \in \mathcal{I}_i} \ell$.

In view of this discussion, we define the entries of the Grassmann tensor as

$$(4.9) \quad \mathbf{T}_{\mathcal{I}_1, \dots, \mathcal{I}_m} = (-1)^{N+1+\sum \mathcal{I}_1 + \dots + \sum \mathcal{I}_m} \det(A_1^\top[:, \mathcal{I}_1] \dots A_m^\top[:, \mathcal{I}_m]),$$

and conclude the following result:

THEOREM 4.1 ([91]). *Given surjective linear projections $C_i : \mathbb{P}^N \dashrightarrow \mathbb{P}^{n_i}$ for $i = 1, \dots, m$ and $c_i \in \mathbb{Z}$ such that $1 \leq c_i \leq n_i$ and $c_1 + \dots + c_m = N+1$, define the set of corresponding subspaces by (4.4). Up to Zariski closure, this is an algebraic hypersurface cut out in primal Plücker coordinates by \mathbf{T} in (4.9).*

4.3.7. Beyond four cameras. When $N = 3$ and there are $m > 4$ pinhole cameras, a tensor-based model for camera configurations is no longer possible since there is no suitable tuple of codimensions (c_1, \dots, c_m) for the Grassmann tensor construction.

The issue is that various embedded subvarieties that one may associate with the cameras are not hypersurfaces, and thus not specified by a single equation. However models for camera configurations still exist inside appropriate *Hilbert schemes*. Roughly speaking, a Hilbert scheme is the set of ideals of a fixed polynomial ring with a prescribed number of equations in each degree. In particular, one can associate (C_1, \dots, C_m) modulo G to the ideal of its multiview variety \mathcal{M}_C , viewed as a

point in a suitable Hilbert scheme [8]. Aholt, Thomas and Sturmfels [8] proved that this association is generically one-to-one if $m > 2$. The Hilbert scheme approach was recently extended by Lieblich and Van Meter [130] via functorial methods. Their work has the benefit of incorporating calibrated cameras as well.

A rather different line of work encodes the configuration of m cameras through their *viewing graph*. The graph has m vertices, one for each camera. There is an edge between two vertices if the relative position of the two corresponding cameras is known. The edge is then labeled with the fundamental matrix of the camera pair. In most practical scenarios with many cameras, the viewing graph is incomplete. The structure of the graph then determines if the given fundamental matrices are generically sufficient to recover the global camera configuration [176, 11].

5. 3D reconstruction

In this section, we discuss the role that multiview geometry plays in 3D reconstruction algorithms and how zero-dimensional polynomial systems arise. The next section will focus on methods that are used to solve these polynomials with sufficient speed.

5.1. Structure-from-motion pipeline. We have introduced the structure-from-motion problem already in Section 1. Here, we give more detailed algorithmic steps to solve this 3D reconstruction problem. Figure 4 overviews the usual *incremental structure-from-motion pipeline*; see [26] for a full description.

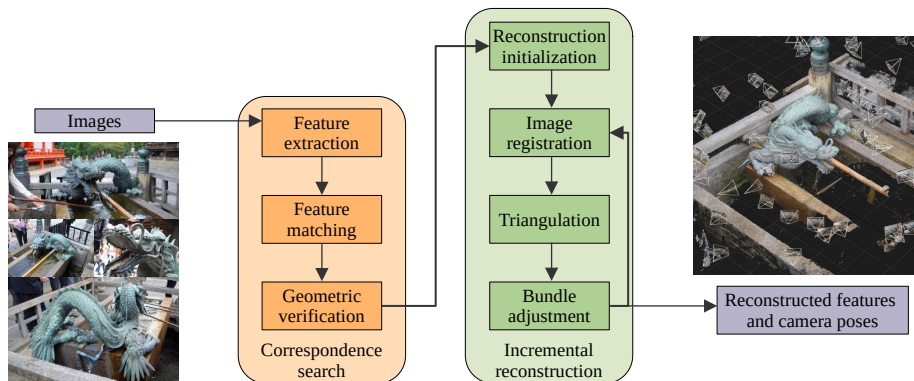


FIGURE 4. Incremental structure-from-motion pipeline.

Feature extraction. The first step in the pipeline is to detect distinguished points or lines (or possibly other information such as conics) in each given image. A standard algorithm is the Scale-Invariant Feature Transform (SIFT) due to Lowe [132].

Feature matching. Next, the detected features are matched across different images; cf. Figure 1b. In particular, feature matching identifies which images show a common part of the scene.

Geometric verification. Typically, not all feature matches from the feature matching step will be correct; many will be outliers. For two (or more) images

with matched features, the geometric verification step tries to compute a geometric transformation that correctly maps sufficiently many features between the images. If such a transformation can be found, the pair (or tuple) of images and their common features that could be mapped are considered to be geometrically verified. For instance, the fundamental (see Section 4.3.1) or essential matrix (see Section 4.3.2) encode the relative pose of two pinhole cameras and thus provide the desired transformation between their two images. The output of the geometric verification step is the viewing graph whose nodes are images and whose (hyper-)edges connect geometrically verified image pairs (or tuples). The (hyper-)edges are labeled with the computed geometric transformations. See Section 4.3.7 for more on the viewing graph.

Since geometric verification forgets the original images and only works with the feature matches from feature matching (see Figure 1c), its core is an algebro-geometric problem that amounts to solving systems of polynomial equations. However, due to the presence of outliers, this step must use robust estimation techniques, usually RANSAC (Random Sample Consensus). More details are in Section 5.2.

Reconstruction initialization. This step picks a starting pair (or tuple) of geometrically verified images (typically, in a dense area of the viewing graph), marks them as *registered*, and reconstructs the 3D coordinates of their matched features (as shown in Figure 1c). Note that the relative pose of the cameras was already precomputed in the previous step.

Image registration. This is the first step of the incremental reconstruction phase. It registers one new image that is connected with previously registered images in the viewing graph by (re-)calculating its camera pose relative to the reconstructed camera poses of the registered images. This can be either done from matched 2D features (as in the geometric verification step) or from 2D-3D correspondences if some of the already reconstructed 3D features are detected 2D features on the new image. Both ways solve a system of polynomial equations, but the latter problem – known as *Perspective-n-Point (PnP)* if all detected features are points – can be typically solved faster.

Triangulation. This step reconstructs the 3D coordinates of all features that the newly registered image has in common with any of the previously registered images (except, of course, for those features whose 3D coordinates were reconstructed before); see Section 3.2.

Bundle adjustment. This step refines the 3D features and camera poses reconstructed so far to minimize the accumulation of errors in the incremental reconstruction phase; see [179] for more details. Afterward, a new image will be registered and the incremental reconstruction phase repeats until (almost) all cameras and sufficiently many 3D features are reconstructed to approximate the 3D scene. Bundle adjustment is a very important step in the pipeline, but a fuller account falls outside our scope. See [147] for another survey article that emphasizes numerical optimization aspects in structure-from-motion more ours does.

5.2. Geometric verification. The algebro-geometric problems within the structure-from-motion pipeline aim to reconstruct the relative camera positions locally. That is, we seek the relative pose for only a few (e.g., two) of the given images at a time, based on feature matches between the images. A salient issue is that some of the purported feature matches will be *completely erroneous*. Indeed feature extraction/matching methods applied to real images invariably produce a

nontrivial fraction of incorrect matches; and the problem becomes severe for scenes with repeated textures (e.g., a brick wall), among others. Therefore reconstruction methods must be robust to outliers. A general paradigm for estimation in the presence of outliers was introduced by Fischler and Bolles [76], who were motivated by the computer vision setting. Their *Random Sample Consensus (RANSAC)* and its subsequent variants remain popular today for computing local reconstructions.

To illustrate RANSAC and show how it motivates solving zero-dimensional polynomial systems in vision, we discuss essential matrix estimation. In this example, data consists of several purported point matches

$$(x_1, y_1), \dots, (x_n, y_n) \in \mathbb{P}_{\mathbb{R}}^2 \times \mathbb{P}_{\mathbb{R}}^2.$$

Let $\mathcal{E} \subset \mathbb{P}(\text{Mat}^{3 \times 3})$ be the variety of essential matrices defined by (4.3). We seek $E \in \mathcal{E}$ which best fits the veridical point pairs amongst the data. By construction, if (x_i, y_i) is a correct (and noiseless) image point pair and E is the ground-truth essential matrix, then

$$y_i^\top E x_i = 0.$$

Notice that this constraint on E is linear and of codimension 1. Thus given $\dim(\mathcal{E}) = 5$ such constraints, we expect up to $\deg(\mathcal{E}) = 10$ real solutions for E . However it is unknown which of the purported points pairs are veridical. RANSAC achieves robust estimation by randomly sampling a subset $\mathcal{I} \subseteq [n] = \{1, \dots, n\}$ of five point pairs and fitting to them exactly by solving the polynomial system:

$$(5.1) \quad \det(E) = 0, \quad EE^\top E - \frac{1}{2} \text{trace}(EE^\top)E = 0, \quad y_i^\top E x_i = 0 \quad (i \in \mathcal{I}).$$

Letting E_1, \dots, E_s be the real solutions, RANSAC checks if there exists a consensus amongst the other $n - 5$ point pairs as to whether any of the solutions agree with most of the other point pairs. RANSAC re-samples \mathcal{I} until a consensus is found. We note that this involves a choice of error metric to measure the agreement between E_k and (x_i, y_i) for $i \in \mathcal{I}$. A simple choice is $(y_i^\top E_k x_i)^2$ often called algebraic error, but often the geometric reprojection error or its first-order approximation called Sampson error are preferred [94]. We also remark that popular variants of RANSAC, like LO-RANSAC [48], polish the winning E_k by using all point pairs in $[n]$ that agree with E_k to form a non-linear least squares cost which is minimized starting from E_k .

5.3. Minimal problems. The polynomial system (5.1) is called a minimal problem in the vision literature, reflecting the fact that (5.1) uses the minimal amount of data such that the solution is uniquely determined up to finitely many solutions. More generally, minimal problems are 3D reconstruction problems such that random input instances have a finite positive number of solutions. Formally, a structure-from-motion problem is *minimal* if the associated joint camera map $\Phi : \mathcal{X} \times \mathcal{C}_m \dashrightarrow \mathcal{Y}$ over the complex numbers has generically finite non-empty fibers, modulo the group G that acts on the fibers. In other words, for a generic (complex) $y \in \mathcal{Y}$, the fiber $\Phi^{-1}(y)$ is non-empty and consists of finitely many G -orbits.

By choosing appropriate coordinates for camera configurations modulo the group G (for example, by using the multifocal tensors in Section 4.3), a minimal problem can be cast as a zero-dimensional parameterized polynomial system. Thus one expects that a minimal problem can be solved efficiently, as long as its generic number of complex solutions is sufficiently small. This generic number of

complex solutions – known as the *algebraic degree* of the minimal problem – is a measure of the minimal problem’s intrinsic difficulty.

EXAMPLE 5.1. Reconstructing five points in general position observed by two calibrated pinhole cameras (see Figure 1c) is a minimal problem. This is because, generically, the system (5.1) has 10 complex solutions (i.e., essential matrices), so 20 complex pairs of cameras (modulo the scaled special Euclidean group), and for each camera pair there are five unique 3D points mapping to the given image points. Note that the number of *real* solutions to (5.1) depends on the image data. The real count is generically amongst $\{0, 2, 4, 6, 8, 10\}$, but varies with the specific five points. In particular, understanding when there exists at least a real solution is subtle [3]. An even more difficult problem is to determine when there is at least one chiral reconstruction, i.e. a real solution where the 3D points lie *in front* of the cameras [155]. If we are given six points in two calibrated views, the system (5.1) no longer corresponds to a minimal problem, as generically there is no complex solution. We need the image data to lie on the *Chow hypersurface* in order for (5.1) to be soluble; see [77] for an explicit Pfaffian formula defining the Chow hypersurface obtained using Ulrich sheaves, or [29] for a simpler construction based on Jordan algebras.

The literature on minimal problems is vast. Many minimal problems have been described, solvers have been developed for them, and new minimal problems are constantly appearing; see e.g. [101, 146, 119, 144, 167, 156, 67, 115, 117, 181, 163, 126, 43, 14, 13, 139, 192, 118, 69].

There are also many variations of the above definition. For instance, when solving 3D reconstruction by RANSAC as described in Section 5.2, one often aims to recover the camera parameters only. Hence, often a structure-from-motion problem is referred to as minimal if for a generic image tuple $y \in \mathcal{Y}$, the projection of the fiber $\Phi^{-1}(y) \subset X \times \mathcal{C}_m$ onto the space \mathcal{C}_m of cameras is non-empty and finite modulo G . In the following, we call such problems *camera-minimal* and reserve the term *minimal* for when we aim to recover the 3D structure in \mathcal{X} as well (as in the definition before Example 5.1). Note that every minimal problem is camera-minimal but not vice versa.

EXAMPLE 5.2. The following problem is camera-minimal (shown in [105] where it is called 3PPP + 1PPL): Reconstruct four points $X_1, X_2, X_3, X_4 \in \mathbb{P}^3$ and a line $L \subset \mathbb{P}^3$ incident to X_4 that are observed by three calibrated pinhole cameras such that the first two cameras see only the four points and the third camera only sees X_1, X_2, X_3 and the line L ; see Figure 5. In fact, it typically has 272 complex solutions in terms of camera parameters. However, this problem is *not* minimal since the line L cannot be recovered uniquely when the three cameras are known: There is a one-dimensional family of lines that yield the same image line in the third view.

In standard structure-from-motion reconstructions, (camera-)minimal problems need to be solved many times to ensure RANSAC finds a solution that is not corrupted by outliers. Thus, minimal solvers need to be fast. Furthermore, they should be accurate, since numerical errors could jeopardize RANSAC’s success as well. We also would like to handle various nearly-degenerate geometries, such as near coplanarities amongst the five point pairs in (5.1), as such situations do arise in natural images. In Section 6, we review the symbolic and numerical minimal solvers that are used to meet these needs.

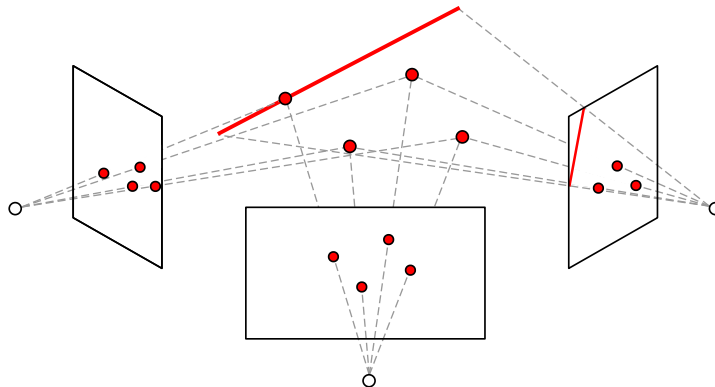


FIGURE 5. A camera-minimal problem with algebraic degree 272.

The large zoo of minimal problems in the literature is motivated by the quest to find reconstruction problems that 1) admit a feasible minimal solver as described above, 2) their necessary input data can be detected by state-of-the-art feature extraction methods, and 3) cover the wide variety of reconstruction applications in computer vision. The latter includes variations of the camera model (see Section 2), of the parameters to be reconstructed, or of the input data (also beyond the structure-from-motion problem we focus on here, e.g. camera pose estimation from known 3D *and* 2D data). We list some of the most classical minimal problems in Table 1.

to be reconstructed	minimal data	degree	references
essential matrix	5 point pairs	10	[143, 57]
fundamental matrix	7 point pairs	3	[87] already known in 19th century [95, 170]
relative pose of 2 calibrated cameras with unknown common focal length	6 point pairs	15	[167]
absolute pose of 1 calibrated camera (P3P, image registration)	3 world-image point pairs	4	[85] already known in 19th century [84]
planar homography	4 point pairs	1	
calibrated planar homography	4 point pairs	12	[64, 75]
trifocal tensor	9 line triples	36	[122]
calibrated trifocal tensor	3 point triples +1 line triple	216	[105]
relative pose of 2 projective cameras with unknown radial lens distortion	8 point pairs	16	[119]
world point under noise (triangulation, reprojection error)	known cameras with: • 1 point pair • 1 point triple	• 6 • 47	[92] [168]

TABLE 1. Some representative minimal problems. Several of these minimal problems are classical and integrated in vision pipelines.

Efforts have been undertaken to provide complete catalogs of some classes of minimal problems. Kileel [105] describes all 66 camera-minimal problems (incl. their algebraic degrees) for three calibrated pinhole cameras that can be formulated using linear constraints on the trifocal tensor. Duff, Kohn, Leykin, and Pajdla [64]

characterize all 30 minimal problems (including their algebraic degrees) of reconstructing points, lines and their incidences for an arbitrary number of calibrated pinhole cameras under the assumption that all points and lines are observed by every camera. In a follow-up work allowing partial visibility [65], they classify all camera-minimal and minimal problems of three calibrated pinhole cameras observing point-line arrangements such that each line is incident to at most one point. In particular, there are 759 (equivalence classes of) camera-minimal problems with algebraic degree less than 300.

6. Polynomial solvers for minimal problems

In this section, we discuss symbolic and numerical methods to construct solvers for minimal problems in computer vision, e.g. the minimal problems in Table 1.

Algebraically, we model a minimal problem as a *zero-dimensional parameterized polynomial system*:

$$(6.1) \quad \begin{cases} f_1(x_1, \dots, x_n; \theta_1, \dots, \theta_t) = 0 \\ \vdots \\ f_k(x_1, \dots, x_n; \theta_1, \dots, \theta_t) = 0. \end{cases}$$

Here $x = (x_1, \dots, x_n)$ are variables, and $\theta = (\theta_1, \dots, \theta_t)$ are parameters (e.g., coming from image point correspondences). The equations f_i are polynomials in both x and θ , typically with integer coefficients (e.g., the epipolar constraints (5.1)). Write \mathcal{I} for the ideal generated by the equations

$$\mathcal{I} = \{p_1 f_1 + \dots + p_k f_k \mid p_i \in \mathbb{R}[x_1, \dots, x_n; \theta_1, \dots, \theta_t]\}.$$

Let $|\theta$ denotes specialization to concrete parameter values $\theta \in \mathbb{R}^t$. Minimality of the problem translates to the following two assumptions:

- A1)** For generic θ , the ideal $\mathcal{I}|\theta$ is zero-dimensional (i.e., has finitely many roots);
- A2)** For generic θ , the ideal $\mathcal{I}|\theta$ is radical (i.e., has no repeated roots)

The conditions imply the existence of a positive integer $N_{\mathbb{C}} = N_{\mathbb{C}}(\mathcal{I})$ such that for generic parameters θ , the number of \mathbb{C} -solutions to (6.1) is $N_{\mathbb{C}}$. Furthermore, each root has multiplicity 1. Note that $N_{\mathbb{C}}$ is the algebraic degree of the minimal problem discussed in Section 5.3.

By definition, a *solver* is meant to receive values for the parameter $\theta \in \mathbb{R}^t$, and then output the set of corresponding real solutions $V_{\mathbb{R}}(\mathcal{I}|\theta) \subset \mathbb{R}^n$ to (6.1). A salient issue to bear in mind is the *online vs. offline* distinction in computer vision: When given a specific parameter value θ , for many vision tasks we must run the solver in real-time. Therefore, online computations must be fast. On the other hand, when developing the solver, we are free to dedicate far more time and computational resources offline.

6.1. Symbolic method: Elimination templates. Currently a symbolic method is the most popular one to build minimal solvers in vision. At the heart of the method is a classical fact that zero-dimensional polynomial systems can be converted to eigenvector problems.¹

¹A different symbolic approach, based instead on *resultants*, is being developed by Bhayani, Heikkilä and Kukulova [24, 25].

LEMMA 6.1. Let $\theta \in \mathbb{R}^t$, and the corresponding solutions to (6.1) be $V_{\mathbb{C}}(\mathcal{I}|\theta) = \{v_1, \dots, v_{N_{\mathbb{C}}}\} \subset \mathbb{C}^n$. Let $P \in \mathbb{R}[x_1, \dots, x_n]$ be a polynomial separating the solutions, that is, $P(v_i) \neq P(v_j)$ for all $i \neq j$. Let $\mathcal{B} = \{b_1, \dots, b_{N_{\mathbb{C}}}\} \subseteq \mathbb{R}[x_1, \dots, x_n]$ be such that its reduction modulo $\mathcal{I}|\theta$ is a vector space basis $\overline{\mathcal{B}} = \{\overline{b}_1, \dots, \overline{b}_{N_{\mathbb{C}}}\}$ of the quotient ring $\mathbb{R}[x_1, \dots, x_n]/\mathcal{I}|\theta$. Multiplication by P is a linear endomorphism on $\mathbb{R}[x_1, \dots, x_n]/\mathcal{I}|\theta$, represented with respect to $\overline{\mathcal{B}}$ by a matrix

$$(6.2) \quad [\text{mult}(P)|_{\theta}]_{\overline{\mathcal{B}}} \in \mathbb{R}^{N_{\mathbb{C}} \times N_{\mathbb{C}}}, \quad \overline{P}b_j := \sum_{i=1}^{N_{\mathbb{C}}} ([\text{mult}(P)|_{\theta}]_{\overline{\mathcal{B}}})_{ij} \overline{b}_i.$$

Then $[\text{mult}(P)|_{\theta}]_{\overline{\mathcal{B}}}$ is diagonalizable with eigenvalue/left eigenvectors pairs given by $(P(v_i), \mathcal{B}(v_i)) \in \mathbb{C} \times \mathbb{C}^{N_{\mathbb{C}}}$ for $i = 1, \dots, N_{\mathbb{C}}$.

In [52], Cox gives an interesting history of Lemma 6.1, which is often (wrongly) attributed to Stickelberger. We call P the *action polynomial* and $[\text{mult}(P)|_{\theta}]_{\overline{\mathcal{B}}}$ the *action matrix*. Notice that if the action matrix is available, then Lemma 6.1 shows how the solutions v_i to (6.1) may be computed: from the eigenvectors w_i of the action matrix we require $\mathcal{B}(v_i)$ to be proportional to w_i . To make the recovery of v_i easy, typically \mathcal{B} is chosen to consist of monomials.

Thus the main challenge is to obtain the action matrix online. In principle, it requires computing identities of the form

$$(6.3) \quad Pb_j = \sum_{i=1}^{N_{\mathbb{C}}} ([\text{mult}(P)|_{\theta}]_{\overline{\mathcal{B}}})_{ij} b_i + \sum_{i=1}^k q_{ij} f_i|_{\theta} \in \mathbb{R}[x_1, \dots, x_n],$$

for $j = 1, \dots, N_{\mathbb{C}}$ where $q_{ij} \in \mathbb{R}[x_1, \dots, x_n]$ and $([\text{mult}(P)|_{\theta}]_{\overline{\mathcal{B}}})_{ij} \in \mathbb{R}$. Gröbner basis computations are too slow to be performed online, and not viable in floating point arithmetic anyways. Instead, the main tool is *elimination templates*.

Fix choices of $\mathcal{B} \subset \mathbb{R}[x_1, \dots, x_n]$ and $P \in \mathbb{R}[x_1, \dots, x_n]$ such that:

- A3)** For generic θ , $\overline{\mathcal{B}} \subset \mathbb{R}[x_1, \dots, x_n]/\mathcal{I}|\theta$ is a vector space basis;
- A4)** For generic θ , P separates $V_{\mathbb{C}}(\mathcal{I}|\theta)$.

In the present setting, elimination templates are defined as follows.

DEFINITION 6.2. A set $\mathcal{E} = \{e_1, \dots, e_T\} \subset \mathcal{I} \subseteq \mathbb{R}[x_1, \dots, x_n; \theta_1, \dots, \theta_t]$ is an *elimination template* if **A5)** For generic θ , we have $P \cdot \mathcal{B} \subset \text{span}(\mathcal{B} \cup \mathcal{E}|\theta)$.

Often \mathcal{E} is chosen to be x -monomials multiplied by f_1, \dots, f_k . By Definition 6.2,

$$(6.4) \quad Pb_j = \sum_{i=1}^{N_{\mathbb{C}}} ([\text{mult}(P)|_{\theta}]_{\overline{\mathcal{B}}})_{ij} b_i + \sum_{\ell=1}^T \star e_{\ell}|_{\theta} \in \mathbb{R}[x_1, \dots, x_n]$$

for $j = 1, \dots, N_{\mathbb{C}}$ and scalars \star . Computing the action matrix thus becomes a linear system. Specifically, fix $\mathcal{C} = \{c_1, \dots, c_M\} \subset \mathbb{R}[x_1, \dots, x_n]$ such that

- A6)** For generic θ , $\mathcal{E}|\theta \subset \text{span}(\mathcal{B} \cup \mathcal{C})$.

Often \mathcal{C} is all x -monomials appearing in any $e_{\ell} \in \mathcal{E}$ with nonzero coefficient in $\mathbb{R}[\theta_1, \dots, \theta_t]$, not already in \mathcal{B} . Form a matrix called the *elimination template matrix*, denoted $[\text{elim}(P)|_{\theta}]_{\mathcal{B}, \mathcal{E}, \mathcal{C}} \in \mathbb{R}^{(T+N_{\mathbb{C}}) \times (N_{\mathbb{C}}+M)}$, with rows indexed by $\mathcal{E}|\theta \cup P \cdot \mathcal{B}$ and columns indexed by $\mathcal{B} \cup \mathcal{C}$:

$$(6.5) \quad \begin{array}{c} e_1|_\theta \\ \vdots \\ e_T|_\theta \\ Pb_1 \\ \vdots \\ Pb_{N_C} \end{array} \left(\begin{array}{cc|cc} b_1 & \dots & b_{N_C} & c_1 & \dots & c_M \\ & & \star & & & \star \\ \hline & & \star & & & \star \end{array} \right),$$

where each entry is the coefficient of the column in the row. Thanks to (6.4), elementary row operations can reduce the elimination template matrix to the form

$$(6.6) \quad \begin{array}{c} e_1|_\theta \\ \vdots \\ e_T|_\theta \\ Pb_1 \\ \vdots \\ Pb_{N_C} \end{array} \left(\begin{array}{cc|cc} b_1 & \dots & b_{N_C} & c_1 & \dots & c_M \\ & & \star & & & \star \\ \hline & & [\text{mult}(P)|_\theta]_{\overline{\mathcal{B}}} & & & \mathbf{0} \end{array} \right).$$

The bottom-left block of (6.6) is the desired action matrix.

The eigenvectors and elimination templates method is summarized in Algorithm 1. In the online part, the most costly step is computing the pseudo-inverse of the top-right block of the elimination template matrix. In the offline phase, we seek $\mathcal{B}, P, \mathcal{E}, \mathcal{C}$ such that the size of the elimination template matrix is as small as possible.

For the offline procedure, full details are beyond our scope but we mention some of the highlights. A breakthrough was obtained by Kukulova, Bujnak and Pajdla in 2008, who showed how find elimination templates automatically, as opposed to by hand [116]. Behind their work, a principle is that “shape” of symbolic calculations should be the same at generic parameters θ , and also preserved if we reduce (6.1) modulo a prime. This enables traditional Gröbner basis computations in the offline phase. In [122] Larsson, Åström and Oskarsson observed that q_{ij} in (6.3) are uniquely defined only up to the first syzygy module of $(f_1|_\theta, \dots, f_k|_\theta)$. Syzygy-reduction [122, Proposition 1] was shown to result in choices of \mathcal{E} with substantially smaller elimination template matrices for many minimal problems. In [123], Larsson, Oskarsson, Åström, Wallis, Kukulova and Pajdla leveraged the fact that the basis \mathcal{B} need not be standard monomials with respect to some Gröbner basis for $\mathcal{I}|_\theta$, only condition **A3** is required (see [140]). The authors chose \mathcal{B} by a random monomial-sampling strategy, and showed the strategy can sometimes produce smaller elimination template matrices than achievable anywhere on the Gröbner fan. Martyushev, Vrablikova and Pajdla further improved the state-of-the-art with a greedy search strategy to reduce the size of \mathcal{C} in [134]. Integrating many of these ideas, Li and Larsson released code for building solvers in [129].

Algorithm 1 Offline/online solver for the parameterized system (6.1)

1: Offline Input
 $\langle f_1, \dots, f_k \rangle \subseteq \mathbb{R}[x_1, \dots, x_n; \theta_1, \dots, \theta_t]$ satisfying **A1-A2**.

2: Offline Precomputations

Find $\mathcal{B} \subseteq \mathbb{R}[x_1, \dots, x_n]$ satisfying **A3**,
 $P \in \mathbb{R}[x_1, \dots, x_n]$ satisfying **A4**,
 $\mathcal{E} \subseteq \mathbb{R}[x_1, \dots, x_n; \theta_1, \dots, \theta_t]$ satisfying **A5**,
 $\mathcal{C} \subseteq \mathbb{R}[x_1, \dots, x_n]$ satisfying **A6**.

Compute the bottom N_C rows of (6.5), and
denote these by $\begin{bmatrix} E_{21} & E_{22} \end{bmatrix} \in \mathbb{R}^{N_C \times (N_C + M)}$.

3: Online Input

Generic $\theta \in \mathbb{R}^t$.

4: Online Computations

Evaluate the top T rows of (6.5) at θ , and
denote these by $\begin{bmatrix} E_{11} & E_{12} \end{bmatrix} \in \mathbb{R}^{T \times (N_C + M)}$.

Thus $[\text{elim}(P)|_{\theta}]_{\mathcal{B}, \mathcal{E}, \mathcal{C}} = \begin{bmatrix} E_{11} & E_{12} \\ E_{21} & E_{22} \end{bmatrix}$.

Compute $E_{21} - E_{22}E_{12}^\dagger E_{11} \in \mathbb{R}^{N_C \times N_C}$.

This equals $[\text{mult}(P)|_{\theta}]_{\overline{\mathcal{B}}}$.

Compute all real eigenvalue/eigenvector pairs
 $(\lambda_1, w_1), \dots, (\lambda_r, w_r) \in \mathbb{R} \times \mathbb{R}^{N_C}$ of $[\text{mult}(P)|_{\theta}]_{\overline{\mathcal{B}}}$.

Determine $v_1, \dots, v_r \in \mathbb{C}^n$ such that
 $P(v_i) = \lambda_i$ and $\mathcal{B}(v_i) \propto w_i$.

5: Online Output
 $V_{\mathbb{R}}(\mathcal{I}|\theta) = \{v_1, \dots, v_r\} \cap \mathbb{R}^n$.

6.2. Numerical method: Homotopy continuation. An alternative method for building minimal problem solver is homotopy continuation. Homotopy continuation [166] is a path-following, ODE-based numerical method to solve parametrized zero-dimensional polynomial systems of a significantly different nature than the eigenvectors and elimination templates method described above. It uses only floating-point arithmetic operations, and exploits the offline vs. online paradigm in a different way.

In the offline phase, homotopy continuation solves one generic instance of the minimal problem (i.e., the polynomial system $f(x; \theta_*) = 0$ for a fixed choice of parameters). The offline solve is done effectively from scratch. Specifically, homotopy continuation chooses a *start system* $g(x) = 0$ of polynomials with the same variables and degree structure as $f(x; \theta_*) = 0$ that is trivial to solve (e.g., the start solutions are roots of unity). Then homotopy continuation interpolates from the start system to the minimal problem instance via linear interpolation:

$$h(x; t) = (1 - t)f(x; \theta_*) + tg(x),$$

as t goes from 1 to 0. During the interpolation, we numerically track how the solutions to $g(x) = 0$ evolve [55, 56]. In general, many solution paths diverge. However the paths with finite limits give all solutions to $f(x; \theta_*) = 0$ [166, Theorem 7.1.1]. The offline procedure is costly: its complexity is driven by the number of solutions to $g(x) = 0$, often exponential in the number of variables.

In the online phase, homotopy continuation also interpolates between polynomial systems. But now it tracks solutions of the precomputed minimal problem instance $f(x; \theta_*) = 0$ to the solutions of the desired instance of the minimal problem (i.e., $f(x; \theta) = 0$ for a different choice of parameters). The complexity of the online phase is driven by the number of solutions to $f(x; \theta_0) = 0$, rather than the number of solutions to $g(x) = 0$. Consequently the online solve is much faster than the offline phase. Indeed, in the online solve we track only N_C many paths, which is the intrinsic algebraic degree of the minimal problem. General-purpose software for homotopy continuation includes Bertini [15], HomotopyContinuation.jl [36], NumericalImplicitization.m2 [45], among others.

In computer vision, homotopy continuation has been used to determine the algebraic degrees of (camera-)minimal problems [105, 64, 65]. Homotopy continuation was also previously suggested as a solver for such problems [97, 114], however for many years it was not seen to be competitive with the elimination templates approach. Recently, homotopy continuation yielded the fastest solver for the minimal structure-from-motion problem shown in Figure 6. For this problem no elimination template matrix of reasonable size could be found by the symbolic method of Section 6.1. However, with homotopy continuation a numerically stable solver was built that runs on the order of a second or less [69]. The minimal problem in Figure 6 has algebraic degree $N_C = 312$, so homotopy continuation tracks 312 paths per online solve. The solver was validated on real-data scenarios where the state-of-the-art pipeline COLMAP [164] failed to find enough point-based features, which also highlights the importance of investigating (camera-)minimal problems that involve not only points but also lines.

More recently, homotopy continuation has been combined with machine learning to build competitive solvers for minimal problems of large algebraic degree: Hruby, Duff, Leykin, and Pajdla [98] achieve fast computational speeds by first using machine learning to pick a single start solution and then tracking that solution to a single solution of the desired target system. The start solution does not come from a fixed start system, but rather determines the start system used for homotopy continuation, meaning that the start system is also learned. Another important advance has been to combine GPU computing with homotopy continuation. This was recently carried out by Chien, Fan, Abdelfattah, Tsigaridas, Tomov and Kimia [46] on various benchmark minimal problems.

7. Degeneracies and discriminants

This section is devoted to degenerate configurations of 3D scenes and cameras. Section 7.1 focuses on configurations that do not admit unique recovery from image data. Degenerate views of 3D curves and surfaces are discussed in Section 7.2. Finally, Section 7.3 outlines the connection between degenerate instances of minimal problems and condition numbers that measure how sensitive numerical reconstruction algorithms are to errors in the input.

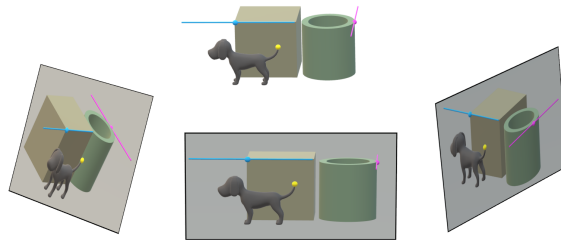


FIGURE 6. A minimal problem with algebraic degree 312: three calibrated pinhole cameras observe three points, two of which have an incident line. Homotopy continuation was used to build a solver for this minimal problem taking 1 second or less, whereas symbolic methods haven't yielded a practical solver [69].

7.1. Critical loci. A *critical configuration* in a structure-from-motion problem is a pair $(X, C) \in \mathcal{X} \times \mathcal{C}_m$ consisting of an ordered subset X of $\mathbb{P}_{\mathbb{R}}^3$ and an m -tuple of cameras C such that the resulting m images $\Phi(X, C)$ do not have a unique reconstruction modulo the group G that acts on the fibers of the joint camera map Φ . In other words, a configuration of 3D points $X \in \mathcal{X}$ and cameras $C \in \mathcal{C}_m$ is critical if there is another configuration $(X', C') \in \mathcal{X} \times \mathcal{C}_m$ that is not in the same G -orbit as (X, C) and produces the same images, i.e., $\Phi(X, C) = \Phi(X', C')$.

The study of critical configurations for two pinhole cameras goes back to the German-Austrian literature on photogrammetry, where critical loci were known as *gefährliche Örter*: Krames [112] showed that an ordered set of 3D points and two pinhole cameras form a critical configuration only if the points and the two camera centers lie on a real ruled quadric surface; see also Maybank [137] for a modern reference. Recall that a quadric surface in $\mathbb{P}_{\mathbb{R}}^3$ is said to be *ruled* if it contains a line. There are four projectively non-equivalent ruled quadrics. They can be distinguished based on the rank of a symmetric matrix $S \in \mathbb{R}^{4 \times 4}$ giving a defining equation $X^T S X = 0$ of the quadric: smooth ruled quadric (rank $S = 4$), cone (rank $S = 3$), two planes (rank $S = 2$), and double plane (rank $S = 1$); see Figure 7.

A first characterization of critical configurations of 3D points and an *arbitrary* number of projective pinhole cameras modulo the group $\text{PGL}(4, \mathbb{R})$ was provided by Hartley and Kahl [89]. In particular, for $m = 2$, they derive:

THEOREM 7.1. *An ordered set of 3D points and two pinhole cameras form a critical configuration modulo $\text{PGL}(4, \mathbb{R})$ if and only if the points and the two camera centers lie on a real ruled quadric surface Q , with the following two exceptions: 1) Q is a cone and both camera centers lie on the same line on Q but not on its vertex, and 2) Q is two planes and the camera centers do not lie on the same plane. Hence, up to projective equivalence, there are eight critical quadrics with two marked camera centers, shown in Figure 7.*

The classification in [89] has some mistakes for three or more cameras. Bråtelund developed new algebraic techniques [33] and corrected the classification for three cameras [32].

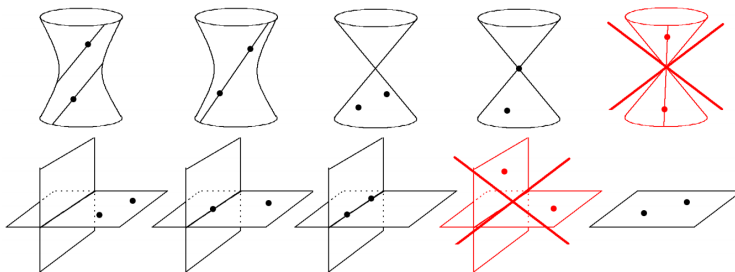


FIGURE 7. The eight critical quadrics (in black) for 3D points and two projective pinhole cameras. The marked points are the camera centers. The exceptions in Theorem 7.1 are red. (Courtesy of Martin Bråtelund.)

Kahl and Hartley [103] also studied the critical configurations of 3D points and calibrated pinhole cameras, modulo the scaled special Euclidean group of \mathbb{R}^3 . They provide a full characterization for two cameras and show the existence of critical configurations for an arbitrary number of points and cameras. It is still an open problem to derive the complete catalog of all critical configurations consisting of 3D points and more than two calibrated pinhole cameras.

REMARK 7.2. Another natural notion of critical locus that is not as prominent in the vision literature as the critical configurations described above is the ramification locus of the joint camera map. For instance, for a minimal problem of algebraic degree larger one, almost all configurations $(X, C) \in \mathcal{X} \times \mathcal{C}_m$ are critical (over \mathbb{C}). However, the ramification locus of the joint camera map of such a minimal problem carries crucial meaning: configurations close to the ramification locus often correspond to ill-conditioned problem instances [41, 58, 59], which has negative algorithmic consequences such as numerical instability; see also Section 7.3.

Critical configurations are also understood in a variety of other settings. Critical loci for 3D lines and three pinhole cameras are for instance investigated by Buchanan [38, 39], Maybank [138], Navab and Faugeras [142], and Zhao and Chung [193]. They are congruences in $\text{Gr}(1, \mathbb{P}^3)$ that can be parametrized by Bordiga surfaces in \mathbb{P}^4 . It would be interesting to generalize those results to more cameras, which is currently open.

Buchanan [37] also described the critical configurations for a single pinhole camera, i.e., for the problem of *camera calibration* where both 3D and image points are known and only the camera parameters are to be recovered. Here the critical 3D points and the camera center lie either on a (possibly reducible but connected) twisted cubic or on the union of a line and a plane such that the camera center lies on the line.

Åström and Kahl [12] classified the critical loci for 1D structure-from-motion problems where 2D points are projected via pinhole cameras of the form $\mathbb{P}^2 \dashrightarrow \mathbb{P}^1$. Critical configurations of 2D points and camera centers lie on cubic curves.

Bertolini, Turrini, and coauthors generalized several of the results above to higher dimensions, i.e., where the classical pinhole cameras $\mathbb{P}^3 \dashrightarrow \mathbb{P}^2$ are replaced by projections $\mathbb{P}^N \dashrightarrow \mathbb{P}^n$, $N > n$; see e.g. [22, 18, 19, 16, 21]. As explained

at the end of Section 4.3, the study of general projections is motivated by the reconstruction of dynamic scenes. Several of their works also perform simulated experiments to test numerical instability phenomena for problem instances near critical loci; see in addition [17, 23, 20].

Despite the literature on critical configurations outlined above, critical loci of vision problems are still unexplored in many settings, e.g. for 3D point-line arrangements or for other camera models besides pinhole cameras.

7.2. Aspect graphs and visual events. In this section, we focus on taking pictures of an algebraic curve or surface X in \mathbb{P}^3 with a pinhole camera $C : \mathbb{P}^3 \dashrightarrow \mathbb{P}^2$. Clearly, if X is a curve, its image is typically a plane curve and we write $Y_C(X)$ for its Zariski closure in \mathbb{P}^2 . If X is a surface, we denote by $Y_C(X)$ its *image contour*, also known as *silhouette* or *outline curve*, in the image plane \mathbb{P}^2 . This is the curve that bounds the two-dimensional region that is the image of the surface X taken by the camera C . In other words, it is the natural sketch one might use to depict the surface; see Figure 8 for an image contour of a torus. Formally, $Y_C(X)$ is the branch locus of the map C restricted to X , i.e., it is the projection of the critical points where viewing lines through the camera center are tangent to the surface X .

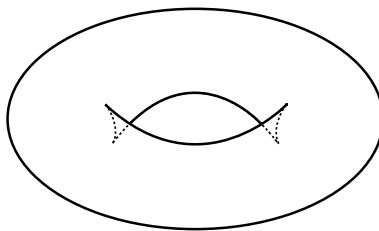


FIGURE 8. Image contour of a torus.

The reconstruction of an algebraic surface from its image contour has been studied intensively, e.g., by Zariski [191], Segre [165], Biggiogero [27, 28], Chisini [47] who conjectured that a surface can be reconstructed from its image contour, Kulikov [120, 121] who solved Chisini's conjecture, and Forsyth [79] who solved the special case of a smooth surface and a general camera. Algorithmic solutions are for instance provided in [113, 54, 80, 81].

The *aspects* of a curve or surface X are the stable views when the camera moves, i.e., where the topology and singularities of the plane curve $Y_C(X)$ do not change under perturbations of the camera center. There is a finite number of aspects and they are the nodes of the *aspect graph*. Its edges are the *visual events* that transition between different aspects. For instance, Figure 8 shows an aspect of a torus, and a visual event occurs when we rotate the torus until the real singularities disappear. The aspect graph was first introduced by Koenderink and van Doorn [109] under the name of *visual potential*. A detailed discussion of image contours and their visual events can be found in Koenderink's book [108].

Although there has not been much use of aspect graphs in real-life applications, they have been an active research topic in the computer vision community; see e.g. Bowyer's and Dyer's survey [31] or Chapter 13 in Forsyth's and Ponce's book [78]. In particular, several algorithms for the computation of aspect graphs of algebraic

surfaces were proposed, using both symbolic and numerical methods [153, 151, 159, 160, 148].

From the algebraic perspective, visual events have been studied by Petitjean [150] and Kohn, Sturmfels, and Trager [111]. The *visual event surface* $\mathcal{V}(X)$ of the curve or surface X is the Zariski closure in \mathbb{P}^3 of the set of camera centers where a visual event occurs. For a curve X in \mathbb{P}^3 , the visual event surface typically has three irreducible components, each representing a different type of visual event. On the image curve $Y_C(X)$, these types correspond to the three Reidemeister moves from knot theory [157]; see Figure 9

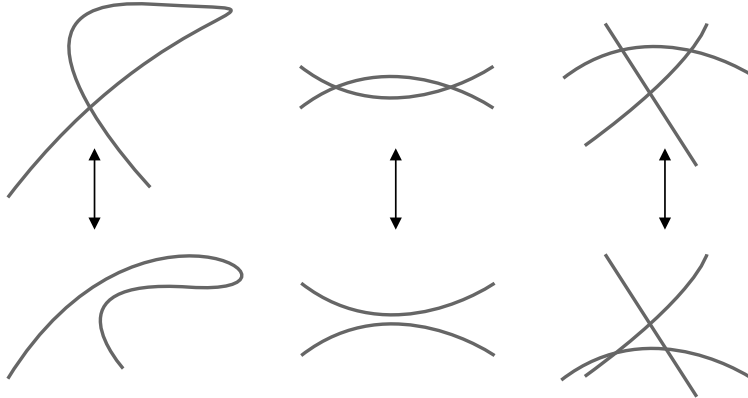


FIGURE 9. The three types of visual events of a space curve.

If X is a surface, its visual event surface $\mathcal{V}(X)$ typically has five irreducible components that arise from six different types of visual events (here two types of events cannot be distinguished algebraically, i.e. they lie on the same component of $\mathcal{V}(X)$, but they represent two distinct behaviors over the real numbers). These six types of events correspond to the non-generic singularities from catastrophe theory [174, 10].

In [111], the components of the visual event surface $\mathcal{V}(X)$ of a curve or surface X are alternatively characterized via the iterated singular loci of the *higher associated hypersurfaces* [82] / *coisotropic hypersurfaces* [110] of X . For a surface X , the coisotropic hypersurfaces are the *dual surface* X^\vee in $(\mathbb{P}^3)^*$ and the *Hurwitz threefold* $\text{Hur}(X)$ in $\text{Gr}(1, \mathbb{P}^3)$, i.e., the Zariski closure of the set of planes (respectively lines) tangent to X . Figure 10 shows the iterated singular loci of these hypersurfaces till the level of curves. The five components of $\mathcal{V}(X)$ are encoded by the curves in the last row of Figure 10: two components are the dual surfaces to the curves on the left. The remaining three components are ruled by the lines on the curves shown in the right diagram.

EXAMPLE 7.3. Consider the curve $\mathcal{F}^\ell(X) \subset \text{Gr}(1, \mathbb{P}^3)$ associated with a surface $X \subset \mathbb{P}^3$ of degree at least four. The curve $\mathcal{F}^\ell(X)$ is the Zariski closure of the set of all lines that intersect the surface X at some point with multiplicity four. Such lines are called *flecnodal*. The union of all flecnodal lines is the *flecnodal surface* of X ; it is one of the irreducible components of the visual event surface $\mathcal{V}(X)$. The visual event corresponding to the flecnodal surface is called *swallowtail event*.

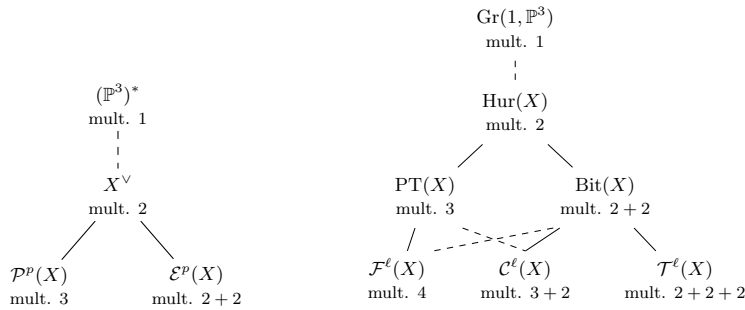


FIGURE 10. Loci of planes and lines that meet a surface X with assigned multiplicities. For instance, “mult. $2 + 2 + 2$ ” on the right-hand side refers to the locus of tritangent lines. A dashed (resp. solid) edge means that the lower variety is contained in (the singular locus of) the upper one [111].

For an explicit example, let us consider the quartic surface parametrized by $(s, t) \mapsto (s, t, s^2 + 3st + t^4)$. The surface is shown in yellow in Figure 11. In Figure 11a, the surface’s image contour is smooth. In Figure 11b, the image contour has two cusps and a node, as illustrated in the torus example in Figure 8. The transition occurs when the camera center is located on a flecnodal line. On a general surface, there is a one-dimensional family of points such that one of the tangent lines at that point is flecnodal. The family makes up the curve shown in red in Figure 11. For the particular surface there, every red point has two flecnodal lines. The lines are shown for a particular point in Figures 11a and 11b, and for many points in Figure 11c.

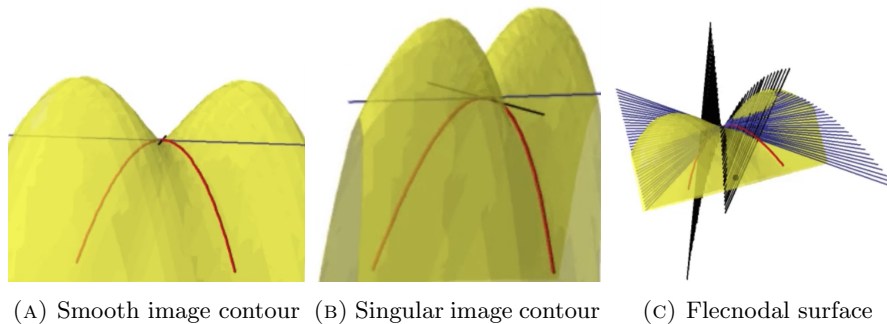


FIGURE 11. Quartic surface parametrized by $(s, t, s^2 + 3st + t^4)$ (in yellow) with flecnodal lines that meet the surface with multiplicity 4 at one of the red points. A swallowtail event happens when the 2 cusps and the node in Figure 11b come together to a higher order singularity.

Similarly, if X is a curve its coisotropic hypersurfaces are the dual surface X^\vee in $(\mathbb{P}^3)^*$ and the *Chow threefold* in $\text{Gr}(1, \mathbb{P}^3)$, that is, the set of lines meeting X . Their (iterated) singular curves give rise to the three components of $\mathcal{V}(X)$ analogously.

The degrees of the components of $\mathcal{V}(X)$ for a general curve or surface X of fixed degree (and genus in the curve case) are classically known; see [111, Theorems 3.1 and 4.1]. Petitjean provided degree formulas for the five components of $\mathcal{V}(X)$ in the surface case [150], but they appeared in fact already in paragraphs 597, 598, 599, 608 and 613 of Salmon’s 1882 book [162].

7.3. Hurwitz hypersurfaces and condition numbers. The minimal problem (5.1) of computing essential matrices consistent with five point pairs admits the following geometric interpretation: We are computing the intersection of the essential variety $\mathcal{E} \subset \mathbb{P}(\mathbb{R}^{3 \times 3})$ with a data-dependent linear subspace $L \subset \mathbb{P}(\mathbb{R}^{3 \times 3})$ of complementary dimension, namely $L = \{x_i y_i^\top : i \in \mathcal{I}\}^\perp$. In numerical algebraic geometry language, we are computing a *witness set* of \mathcal{E} [166, Chapter 13.3]. Several, though not all, minimal problems in computer vision usefully admit such an interpretation. For instance, Kileel [105] describes all 66 minimal problems for three calibrated pinhole cameras that arise from slicing the calibrated trifocal variety \mathcal{T}_{cal} with linear spaces of complementary dimension.

In the applied algebra community, this description has motivated theoretical works on intersecting a fixed variety $Z \subset \mathbb{P}^n$ with varying linear subspaces of complementary dimension. This includes the detailed study of the *Hurwitz hypersurface* $\text{Hur}(Z)$ by Sturmfels [171]. Writing c for the codimension of Z in \mathbb{P}^n and d for its degree, $\text{Hur}(Z)$ is the Zariski closure in $\text{Gr}(c, \mathbb{P}^n)$ of the set of all c -dimensional projective subspaces L of \mathbb{P}^n such that the intersection $Z \cap L$ does not consist of d reduced points. The Hurwitz hypersurface is intimately linked with the *condition number* [41] of the algebraic function $L \mapsto Z \cap L$. That condition number measures how much the intersection $Z \cap L$ changes when L gets perturbed, which is crucial for the understanding of how much numerical computations such as homotopy continuation are affected by errors. Bürgisser showed that the set of *ill-posed* L , i.e. those with infinite condition, is essentially the Hurwitz hypersurface $\text{Hur}(Z)$ and that (almost) all L with large condition are contained in a small tube around $\text{Hur}(Z)$ [40, Corollary 1.10]. Bürgisser’s work follows the general idea that condition numbers are given by the inverse distance to ill-posedness from numerical analysis [59, 58].

Recently there has been work on condition numbers of minimal problems in the more practical setting, where the dependence is in terms of the perturbation of the image data (instead of perturbation of L in the Grassmannian) by Fan, Kileel and Kimia [70, 71]. Their work drew distinctions between criticality (Section 7.1 above) and ill-posedness (when the condition number is infinite), see [71, Section 5]. For the 5- and 7-point problems, the authors derived condition number formulas in terms of certain Jacobian matrices, and they characterized ill-posed world scenes and ill-posed image point pairs geometrically. Furthermore, real-data experiments showed that poor conditioning can actually plague some computer vision data sets.

References

1. Sameer Agarwal, Timothy Duff, Max Lieblich, and Rekha R Thomas, *An atlas for the pinhole camera*, Foundations of Computational Mathematics (2022), 1–51.
2. Sameer Agarwal, Yasutaka Furukawa, Noah Snavely, Ian Simon, Brian Curless, Steven M Seitz, and Richard Szeliski, *Building Rome in a day*, Communications of the ACM **54** (2011), no. 10, 105–112.
3. Sameer Agarwal, Hon-Leung Lee, Bernd Sturmfels, and Rekha Thomas, *On the existence of epipolar matrices*, International Journal of Computer Vision **121** (2017), no. 3, 403–415.

4. Sameer Agarwal, Andrew Pryhuber, Rainer Sinn, and Rekha Thomas, *The chiral domain of a camera arrangement*, Journal of Mathematical Imaging and Vision (2022), 1–20.
5. Sameer Agarwal, Andrew Pryhuber, and Rekha Thomas, *Ideals of the multiview variety*, IEEE Transactions on Pattern Analysis and Machine Intelligence **43** (2019), no. 4, 1279–1292.
6. Chris Aholt, Sameer Agarwal, and Rekha Thomas, *A QCQP approach to triangulation*, European Conference on Computer Vision, Springer, 2012, pp. 654–667.
7. Chris Aholt and Luke Oeding, *The ideal of the trifocal variety*, Mathematics of Computation **83** (2014), no. 289, 2553–2574.
8. Chris Aholt, Bernd Sturmfels, and Rekha Thomas, *A Hilbert scheme in computer vision*, Canadian Journal of Mathematics **65** (2013), no. 5, 961–988.
9. Christopher Aholt, *Polynomials in multiview geometry*, Ph.D. thesis, University of Washington, 2012.
10. Vladimir I Arnol’d, *Catastrophe theory*, Springer-Verlag, 1984.
11. Federica Arrigoni, Andrea Fusiello, Elisa Ricci, and Tomas Pajdla, *Viewing graph solvability via cycle consistency*, Proceedings of the IEEE/CVF International Conference on Computer Vision, 2021, pp. 5540–5549.
12. Kalle Åström and Fredrik Kahl, *Ambiguous configurations for the 1D structure and motion problem*, Journal of Mathematical Imaging and Vision **18** (2003), no. 2, 191–203.
13. Daniel Barath, *Five-point fundamental matrix estimation for uncalibrated cameras*, Proceedings of the IEEE Conference on Computer Vision and Pattern Recognition, 2018, pp. 235–243.
14. Daniel Barath, Tekla Toth, and Levente Hajder, *A minimal solution for two-view focal-length estimation using two affine correspondences*, Proceedings of the IEEE Conference on Computer Vision and Pattern Recognition, 2017, pp. 6003–6011.
15. Daniel J Bates, Andrew J Sommese, Jonathan D Hauenstein, and Charles W Wampler, *Numerically solving polynomial systems with Bertini*, SIAM, 2013.
16. Marina Bertolini, Gian Mario Besana, Roberto Notari, and Cristina Turrini, *Critical loci in computer vision and matrices dropping rank in codimension one*, Journal of Pure and Applied Algebra **224** (2020), no. 12, 106439.
17. Marina Bertolini, GianMario Besana, and Cristina Turrini, *Instability of projective reconstruction from 1-view near critical configurations in higher dimensions*, International Conference on Midwest Algebra, Geometry and Their Interactions, American Mathematical Society, 2007, pp. 1–12.
18. ———, *Critical loci for projective reconstruction from multiple views in higher dimension: A comprehensive theoretical approach*, Linear Algebra and its Applications **469** (2015), 335–363.
19. Marina Bertolini and Luca Magri, *Critical hypersurfaces and instability for reconstruction of scenes in high dimensional projective spaces*, Machine Graphics and Vision **29** (2020), no. 1/4, 3–20.
20. Marina Bertolini, Luca Magri, and Cristina Turrini, *Critical loci for two views reconstruction as quadratic transformations between images*, Journal of Mathematical Imaging and Vision **61** (2019), no. 9, 1322–1328.
21. Marina Bertolini, Roberto Notari, and Cristina Turrini, *Smooth determinantal varieties and critical loci in multiview geometry*, Collectanea Mathematica **73** (2022), no. 3, 457–475.
22. Marina Bertolini and Cristina Turrini, *Critical configurations for 1-view in projections from $\mathbb{P}^k \rightarrow \mathbb{P}^2$* , Journal of Mathematical Imaging and Vision **27** (2007), no. 3, 277–287.
23. Marina Bertolini, Cristina Turrini, and GianMario Besana, *Instability of projective reconstruction of dynamic scenes near critical configurations*, Proceedings of the IEEE International Conference on Computer Vision, 2007, pp. 1–7.
24. Snehal Bhayani, Janne Heikkilä, and Zuzana Kukelova, *Sparse resultant based minimal solvers in computer vision and their connection with the action matrix*, arXiv preprint arXiv:2301.06443 (2023).
25. Snehal Bhayani, Zuzana Kukelova, and Janne Heikkilä, *A sparse resultant based method for efficient minimal solvers*, Proceedings of the IEEE/CVF Conference on Computer Vision and Pattern Recognition, 2020, pp. 1770–1779.
26. Simone Bianco, Gianluigi Ciocca, and Davide Marelli, *Evaluating the performance of structure from motion pipelines*, Journal of Imaging **4** (2018), no. 8, 98.

27. G Masotti Biggiogero, *La caratterizzazione della curva di diramazione dei piani tripli, ottenuta mediante sistemi di curve pluritangenti*, Ist. Lombardo Sci. Lett. Rend Cl. Sci. Mat. Nat **80** (1947), 151–160.
28. ———, *Sulla caratterizzazione della curva di diramazione dei piani quadrupli generali*, Ist. Lombardo Sci. Lett. Rend Cl. Sci. Mat. Nat **80** (1947), 269–280.
29. Arthur Bik, Henrik Eisenmann, and Bernd Sturmfels, *Jordan algebras of symmetric matrices*, Le Matematiche **76** (2021), no. 2, 337–353.
30. Mireille Boutin and Pierre-Louis Bazin, *Structure from motion: A new look from the point of view of invariant theory*, SIAM Journal on Applied Mathematics **64** (2004), no. 4, 1156–1174.
31. Kevin W Bowyer and Charles R Dyer, *Aspect graphs: An introduction and survey of recent results*, International Journal of Imaging Systems and Technology **2** (1990), no. 4, 315–328.
32. Martin Bråtelund, *Critical configurations for three projective views*, arXiv preprint arXiv:2112.05478 (2021).
33. ———, *Critical configurations for two projective views, a new approach*, Journal of Symbolic Computation **120** (2024), 102226.
34. Paul Breiding, Tü rkü Ö zlü m Ç elik, Timothy Duff, Alexander Heaton, Aida Maraj, Anna-Laura Sattelberger, Lorenzo Venturello, and Oğ uzhan Yürük, *Nonlinear algebra and applications*, Numerical Algebra, Control and Optimization (2021).
35. Paul Breiding, Felix Rydell, Elima Shehu, and Angélica Torres, *Line multiview varieties*, SIAM Journal on Applied Algebra and Geometry **7** (2023), no. 2, 470–504.
36. Paul Breiding and Sascha Timme, *HomotopyContinuation.jl: A package for homotopy continuation in Julia*, International Congress on Mathematical Software, Springer, 2018, pp. 458–465.
37. Thomas Buchanan, *The twisted cubic and camera calibration*, Computer Vision, Graphics, and Image Processing **42** (1988), no. 1, 130–132.
38. ———, *Critical sets for 3D reconstruction using lines*, European Conference on Computer Vision, Springer, 1992, pp. 730–738.
39. ———, *On the critical set for photogrammetric reconstruction using line tokens in $\mathbb{P}_3(\mathbb{C})$* , Geometriae Dedicata **44** (1992), no. 2, 223–232.
40. Peter Bü rgisser, *Condition of intersecting a projective variety with a varying linear subspace*, SIAM Journal on Applied Algebra and Geometry **1** (2017), no. 1, 111–125.
41. Peter Bü rgisser and Felipe Cucker, *Condition: The geometry of numerical algorithms*, Grundlehren der mathematischen Wissenschaften, vol. 349, Springer Science & Business Media, 2013.
42. Eugenio Calabi, Peter J Olver, Chehrzad Shakiban, Allen Tannenbaum, and Steven Haker, *Differential and numerically invariant signature curves applied to object recognition*, International Journal of Computer Vision **26** (1998), 107–135.
43. Federico Camposeco, Torsten Sattler, and Marc Pollefeys, *Minimal solvers for generalized pose and scale estimation from two rays and one point*, European Conference on Computer Vision, Springer, 2016, pp. 202–218.
44. Luca Carlone, *Estimation contracts for outlier-robust geometric perception*, Foundations and Trends® in Robotics **11** (2023), no. 2-3, 90–224.
45. Justin Chen and Joe Kileel, *Numerical implicitization*, Journal of Software for Algebra and Geometry **9** (2019), no. 1, 55–63.
46. Chiang-Heng Chien, Hongyi Fan, Ahmad Abdelfattah, Elias Tsigaridas, Stanimire Tomov, and Benjamin Kimia, *GPU-based homotopy continuation for minimal problems in computer vision*, Proceedings of the IEEE/CVF Conference on Computer Vision and Pattern Recognition, 2022, pp. 15765–15776.
47. Oscar Chisini, *Sulla identità birazionale di due funzioni algebriche di più variabili, dotate di una medesima varietà di diramazione*, Ist. Lombardo Sci. Lett. Rend. Cl. Sci. Mat. Nat.,(3) **80** (1947), 3–6.
48. Ondř ej Chum, Jiří Matas, and Josef Kittler, *Locally optimized RANSAC*, Joint Pattern Recognition Symposium, Springer, 2003, pp. 236–243.
49. Yairon Cid-Ruiz, Oliver Clarke, and Fatemeh Mohammadi, *A study of nonlinear multiview varieties*, Journal of Algebra **620** (2023), 363–391.
50. Diego Cifuentes, Sameer Agarwal, Pablo Parrilo, and Rekha Thomas, *On the local stability of semidefinite relaxations*, Mathematical Programming **193** (2022), no. 2, 629–663.

51. David Cox, John Little, and Donal O’Shea, *Ideals, varieties, and algorithms: An introduction to computational algebraic geometry and commutative algebra*, Springer Science & Business Media, 2013.
52. David A Cox, *Stickelberger and the eigenvalue theorem*, *Commutative Algebra*, Springer, 2021, pp. 283–298.
53. Yuchao Dai, Hongdong Li, and Laurent Kneip, *Rolling shutter camera relative pose: Generalized epipolar geometry*, *Proceedings of the IEEE Conference on Computer Vision and Pattern Recognition*, 2016, pp. 4132–4140.
54. Jean d’Almeida, *Courbe de ramification de la projection sur \mathbb{P}^2 d’une surface de \mathbb{P}^3* , *Duke Mathematical Journal* **65** (1992), no. 2, 229–233.
55. D F Davidenko, *On a new method of numerical solution of systems of nonlinear equations (in Russian)*, *Doklady Akademii Nauk SSSR*, vol. 88, 1953, pp. 601–602.
56. ———, *On the approximate solution of systems of nonlinear equations (in Russian)*, *Ukrains’kyi Matematychnyi Zhurnal* **5** (1953), no. 2, 196–206.
57. Michel Demazure, *Sur deux problèmes de reconstruction*, Tech. Report 882, *INRIA*, 1988.
58. James Weldon Demmel, *On condition numbers and the distance to the nearest ill-posed problem*, *Numerische Mathematik* **51** (1987), no. 3, 251–289.
59. ———, *The geometry of ill-conditioning*, *Journal of Complexity* **3** (1987), no. 2, 201–229.
60. Tim Dobbert, *Matchmoving: The invisible art of camera tracking*, Sybex, 2005.
61. Jan Draisma, Emil Horobeț, Giorgio Ottaviani, Bernd Sturmfels, and Rekha Thomas, *The Euclidean distance degree of an algebraic variety*, *Foundations of Computational Mathematics* **16** (2016), no. 1, 99–149.
62. Dmitriy Drusvyatskiy, Hon-Leung Lee, Giorgio Ottaviani, and Rekha Thomas, *The Euclidean distance degree of orthogonally invariant matrix varieties*, *Israel Journal of Mathematics* **221** (2017), no. 1, 291–316.
63. Dmitriy Drusvyatskiy, Hon-Leung Lee, and Rekha Thomas, *Counting real critical points of the distance to orthogonally invariant matrix sets*, *SIAM Journal on Matrix Analysis and Applications* **36** (2015), no. 3, 1360–1380.
64. Timothy Duff, Kathlén Kohn, Anton Leykin, and Tomas Pajdla, *PLMP – Point-line minimal problems in complete multi-view visibility*, *Proceedings of the IEEE/CVF International Conference on Computer Vision*, 2019, pp. 1675–1684.
65. ———, *PL₁P – Point-line minimal problems under partial visibility in three views*, *European Conference on Computer Vision*, Springer, 2020, pp. 175–192.
66. Timothy Duff, Viktor Korotynskiy, Tomas Pajdla, and Margaret H Regan, *Galois/monodromy groups for decomposing minimal problems in 3D reconstruction*, *SIAM Journal on Applied Algebra and Geometry* **6** (2022), no. 4, 740–772.
67. Ali Elqursh and Ahmed Elgammal, *Line-based relative pose estimation*, *Proceedings of the IEEE Conference on Computer Vision and Pattern Recognition*, 2011, pp. 3049–3056.
68. Laura Escobar and Allen Knutson, *The multidegree of the multi-image variety*, *Combinatorial Algebraic Geometry*, Springer, 2017, pp. 283–296.
69. Ricardo Fabbri, Timothy Duff, Hongyi Fan, Margaret H Regan, David da Costa de Pinho, Elias Tsigaridas, Charles W Wampler, Jonathan D Hauenstein, Peter J Giblin, Benjamin Kimia, et al., *TRPLP – Trifocal relative pose from lines at points*, *Proceedings of the IEEE/CVF Conference on Computer Vision and Pattern Recognition*, 2020, pp. 12073–12083.
70. Hongyi Fan, Joe Kileel, and Benjamin Kimia, *On the instability of relative pose estimation and RANSAC’s role*, *Proceedings of the IEEE/CVF Conference on Computer Vision and Pattern Recognition*, 2022, pp. 8935–8943.
71. ———, *Condition numbers in multiview geometry, instability in relative pose estimation, and RANSAC*, arXiv preprint arXiv:2310.02719 (2023).
72. Xiaodong Fan and René Vidal, *The space of multibody fundamental matrices: Rank, geometry and projection*, *Dynamical Vision*, Springer, 2006, pp. 1–17.
73. Olivier Faugeras and Quang-Tuan Luong, *The geometry of multiple images: The laws that govern the formation of multiple images of a scene and some of their applications*, MIT press, 2001.
74. Olivier Faugeras and Bernard Mourrain, *On the geometry and algebra of the point and line correspondences between n images*, *Proceedings of IEEE International Conference on Computer Vision*, 1995, pp. 951–956.

75. Olivier D Faugeras and Francis Lustman, *Motion and structure from motion in a piecewise planar environment*, International Journal of Pattern Recognition and Artificial Intelligence **2** (1988), no. 03, 48–508.
76. Martin A Fischler and Robert C Bolles, *Random sample consensus: a paradigm for model fitting with applications to image analysis and automated cartography*, Communications of the ACM **24** (1981), no. 6, 381–395.
77. Gunnar Fløystad, Joe Kileel, and Giorgio Ottaviani, *The Chow form of the essential variety in computer vision*, Journal of Symbolic Computation **86** (2018), 97–119.
78. David Forsyth and Jean Ponce, *Computer vision: A modern approach*, 2 ed., Pearson, 2012.
79. David A Forsyth, *Recognizing algebraic surfaces from their outlines*, International Journal of Computer Vision **18** (1996), no. 1, 21–40.
80. Matteo Gallet, Niels Lubbes, Josef Schicho, and Jan Vrsek, *Reconstruction of surfaces with ordinary singularities from their silhouettes*, SIAM Journal on Applied Algebra and Geometry **3** (2019), no. 3, 472–506.
81. Matteo Gallet, Niels Lubbes, Josef Schicho, and Jan Vršek, *Reconstruction of rational ruled surfaces from their silhouettes*, Journal of Symbolic Computation **104** (2021), 366–380.
82. Israel M Gelfand, Mikhail M Kapranov, and Andrei V Zelevinsky, *Discriminants, resultants, and multidimensional determinants*, Birkhäuser, 1994.
83. Giorgio Grisetti, Rainer Kümmerle, Cyrill Stachniss, and Wolfram Burgard, *A tutorial on graph-based SLAM*, IEEE Intelligent Transportation Systems Magazine **2** (2010), no. 4, 31–43.
84. Johann August Grunert, *Das Pothenot'sche problem in erweiterter gestalt; nebst bemerkungen über seine anwendung in der geodäsie*, Grunerts Archiv für Mathematik und Physik (1841), 238–248.
85. Bert M Haralick, Chung-Nan Lee, Karsten Ottenberg, and Michael Nölle, *Review and analysis of solutions of the three point perspective pose estimation problem*, International Journal of Computer Vision **13** (1994), no. 3, 331–356.
86. Corey Harris and Daniel Lowengrub, *The Chern-Mather class of the multiview variety*, Communications in Algebra **46** (2018), no. 6, 2488–2499.
87. Richard Hartley, *Projective reconstruction and invariants from multiple images*, IEEE Transactions on Pattern Analysis and Machine Intelligence **16** (1994), no. 10, 1036–1041.
88. ———, *Chirality*, International Journal of Computer Vision **26** (1998), 41–61.
89. Richard Hartley and Fredrik Kahl, *Critical configurations for projective reconstruction from multiple views*, International Journal of Computer Vision **71** (2007), no. 1, 5–47.
90. ———, *Optimal algorithms in multiview geometry*, Asian Conference on Computer Vision, Springer, 2007, pp. 13–34.
91. Richard Hartley and Frederik Schaffalitzky, *Reconstruction from projections using Grassmann tensors*, International Journal of Computer Vision **83** (2009), no. 3, 274–293.
92. Richard Hartley and Peter Sturm, *Triangulation*, Computer Vision and Image Understanding **68** (1997), no. 2, 146–157.
93. Richard Hartley and René Vidal, *The multibody trifocal tensor: Motion segmentation from 3 perspective views*, Proceedings of the IEEE Conference on Computer Vision and Pattern Recognition, 2004.
94. Richard Hartley and Andrew Zisserman, *Multiple view geometry in computer vision*, 2nd ed., Cambridge, 2003.
95. Otto Hesse, *Die cubische gleichung, von welcher die lösung des problems der homographie von M. Chasles abhängt.*, Journal für die reine und angewandte Mathematik **62** (1863).
96. Anders Heyden and Kalle Åström, *Algebraic properties of multilinear constraints*, Mathematical Methods in the Applied Sciences **20** (1997), no. 13, 1135–1162.
97. Berthold KP Horn, *Relative orientation revisited*, Journal of the Optical Society of America A **8** (1991), no. 10, 1630–1638.
98. Petr Hruby, Timothy Duff, Anton Leykin, and Tomas Pajdla, *Learning to solve hard minimal problems*, Proceedings of the IEEE/CVF Conference on Computer Vision and Pattern Recognition, 2022, pp. 5532–5542.
99. Kun Huang, Robert Fossum, and Yi Ma, *Generalized rank conditions in multiple view geometry with applications to dynamical scenes*, European Conference on Computer Vision, Springer, 2002, pp. 201–216.

100. Atsushi Ito, Makoto Miura, and Kazushi Ueda, *Projective reconstruction in algebraic vision*, Canadian Mathematical Bulletin **63** (2020), no. 3, 592–609.
101. Björn Johansson, Magnus Oskarsson, and Kalle Åström, *Structure and motion estimation from complex features in three views*, Indian Conference on Computer Vision, Graphics and Image Processing, 2002.
102. Michael Joswig, Joe Kileel, Bernd Sturmfels, and André Wagner, *Rigid multiview varieties*, International Journal of Algebra and Computation **26** (2016), no. 04, 775–788.
103. Fredrik Kahl and Richard Hartley, *Critical curves and surfaces for Euclidean reconstruction*, European Conference on Computer Vision, Springer, 2002, pp. 447–462.
104. Fredrik Kahl and Didier Henrion, *Globally optimal estimates for geometric reconstruction problems*, International Journal of Computer Vision **74** (2007), no. 1, 3–15.
105. Joe Kileel, *Minimal problems for the calibrated trifocal variety*, SIAM Journal on Applied Algebra and Geometry **1** (2017), no. 1, 575–598.
106. Joe Kileel, Zuzana Kukelova, Tomas Pajdla, and Bernd Sturmfels, *Distortion varieties*, Foundations of Computational Mathematics **18** (2018), no. 4, 1043–1071.
107. Midori Kitagawa and Brian Windsor, *MoCap for artists: Workflow and techniques for motion capture*, Focal Press, 2008.
108. Jan J Koenderink, *Solid shape*, MIT press, 1990.
109. Jan J Koenderink and Andrea J Van Doorn, *The internal representation of solid shape with respect to vision*, Biological Cybernetics **32** (1979), no. 4, 211–216.
110. Kathlén Kohn and James C Mathews Jr, *Isotropic and coisotropic subvarieties of Grassmannians*, Advances in Mathematics **377** (2021), 107492.
111. Kathlén Kohn, Bernd Sturmfels, and Matthew Trager, *Changing views on curves and surfaces*, Acta Mathematica Vietnamica **43** (2018), no. 1, 1–29.
112. Josef Krames, *Zur ermittlung eines objektes aus zwei perspektiven. (Ein beitrage zur theorie der "gefährlichen örter".)*, Monatshefte für Mathematik und Physik **49** (1941), no. 1, 327–354.
113. David J Kriegman and Jean Ponce, *On recognizing and positioning curved 3-D objects from image contours*, IEEE Transactions on Pattern Analysis and Machine Intelligence **12** (1990), no. 12, 1127–1137.
114. ———, *Geometric modeling for computer vision*, Curves and Surfaces in Computer Vision and Graphics II, vol. 1610, International Society for Optics and Photonics, 1992, pp. 250–260.
115. Yubin Kuang and Kalle Åström, *Pose estimation with unknown focal length using points, directions and lines*, Proceedings of the IEEE International Conference on Computer Vision, 2013, pp. 529–536.
116. Zuzana Kukelova, Martin Bujnak, and Tomas Pajdla, *Automatic generator of minimal problem solvers*, European Conference on Computer Vision, Springer, 2008, pp. 302–315.
117. Zuzana Kukelova, Jan Heller, Martin Bujnak, Andrew Fitzgibbon, and Tomas Pajdla, *Efficient solution to the epipolar geometry for radially distorted cameras*, Proceedings of the IEEE International Conference on Computer Vision, 2015, pp. 2309–2317.
118. Zuzana Kukelova, Joe Kileel, Bernd Sturmfels, and Tomas Pajdla, *A clever elimination strategy for efficient minimal solvers*, Proceedings of the IEEE Conference on Computer Vision and Pattern Recognition, 2017, pp. 4912–4921.
119. Zuzana Kukelova and Tomas Pajdla, *A minimal solution to the autocalibration of radial distortion*, Proceedings of the IEEE Conference on Computer Vision and Pattern Recognition, 2007, pp. 1–7.
120. Victor Stepanovich Kulikov, *On Chisini's conjecture*, Izvestiya Rossiiskoi Akademii Nauk. Seriya Matematicheskaya **763** (1999), 83–116.
121. ———, *On Chisini's conjecture. II*, Izvestiya Rossiiskoi Akademii Nauk. Seriya Matematicheskaya **72** (2008), 63–76.
122. Viktor Larsson, Kalle Åström, and Magnus Oskarsson, *Efficient solvers for minimal problems by syzygy-based reduction*, Proceedings of the IEEE Conference on Computer Vision and Pattern Recognition, 2017, pp. 820–829.
123. Viktor Larsson, Magnus Oskarsson, Kalle Åström, Alge Wallis, Zuzana Kukelova, and Tomas Pajdla, *Beyond Gröbner bases: Basis selection for minimal solvers*, Proceedings of the IEEE Conference on Computer Vision and Pattern Recognition, 2018, pp. 3945–3954.

124. Viktor Larsson, Nicolas Zobernig, Kasim Taskin, and Marc Pollefeys, *Calibration-free structure-from-motion with calibrated radial trifocal tensors*, European Conference on Computer Vision, Springer, 2020, pp. 382–399.
125. Stéphane Laveau and Olivier Faugeras, *Oriented projective geometry for computer vision*, European Conference on Computer Vision, Springer, 1996, pp. 147–156.
126. Gim Hee Lee, *A minimal solution for non-perspective pose estimation from line correspondences*, European Conference on Computer Vision, Springer, 2016, pp. 170–185.
127. Gilad Lerman and Yunpeng Shi, *Robust group synchronization via cycle-edge message passing*, Foundations of Computational Mathematics (2021), 1–77.
128. Binglin Li, *Images of rational maps of projective spaces*, International Mathematics Research Notices **2018** (2018), no. 13, 4190–4228.
129. Bo Li and Viktor Larsson, *Gaps: Generator for automatic polynomial solvers*, arXiv preprint arXiv:2004.11765 (2020).
130. Max Lieblich and Lucas Van Meter, *Two Hilbert schemes in computer vision*, SIAM Journal on Applied Algebra and Geometry **4** (2020), no. 2, 297–321.
131. H Christopher Longuet-Higgins, *A computer algorithm for reconstructing a scene from two projections*, Nature **293** (1981), no. 5828, 133–135.
132. David G Lowe, *Distinctive image features from scale-invariant keypoints*, International Journal of Computer Vision **60** (2004), no. 2, 91–110.
133. Yi Ma, Stefano Soatto, Jana Košecká, and Shankar Sastry, *An invitation to 3-D vision: From images to geometric models*, Interdisciplinary Applied Mathematics, vol. 26, Springer, 2004.
134. Evgeniy Martynushev, Jana Vrablekova, and Tomas Pajdla, *Optimizing elimination templates by greedy parameter search*, Proceedings of the IEEE/CVF Conference on Computer Vision and Pattern Recognition, 2022, pp. 15754–15764.
135. Evgeniy V Martynushev, *On some properties of calibrated trifocal tensors*, Journal of Mathematical Imaging and Vision **58** (2017), no. 2, 321–332.
136. Laurentiu G Maxim, Jose I Rodriguez, and Botong Wang, *Euclidean distance degree of the multiview variety*, SIAM Journal on Applied Algebra and Geometry **4** (2020), no. 1, 28–48.
137. Stephen Maybank, *Theory of reconstruction from image motion*, Springer Series in Information Sciences, Springer Berlin, Heidelberg, 1993.
138. ———, *The critical line congruence for reconstruction from three images*, Applicable Algebra in Engineering, Communication and Computing **6** (1995), no. 2, 89–113.
139. Pedro Miraldo, Tiago Dias, and Srikumar Ramalingam, *A minimal closed-form solution for multi-perspective pose estimation using points and lines*, European Conference on Computer Vision, Springer, 2018, pp. 474–490.
140. Bernard Mourrain, *A new criterion for normal form algorithms*, International Symposium on Applied Algebra, Algebraic Algorithms, and Error-Correcting Codes, Springer, 1999, pp. 430–442.
141. David Mumford, John Fogarty, and Frances Kirwan, *Geometric invariant theory*, Ergebnisse der Mathematik und ihrer Grenzgebiete. 2. Folge, vol. 34, Springer Science & Business Media, 1994.
142. Nassir Navab and Olivier Faugeras, *The critical sets of lines for camera displacement estimation: A mixed Euclidean-projective and constructive approach*, International Journal of Computer Vision **23** (1997), no. 1, 17–44.
143. David Nistér, *An efficient solution to the five-point relative pose problem*, IEEE Transactions on Pattern Analysis and Machine Intelligence **26** (2004), no. 6, 756–770.
144. David Nistér and Henrik Stewénius, *A minimal solution to the generalised 3-point pose problem*, Journal of Mathematical Imaging and Vision **27** (2007), no. 1, 67–79.
145. Luke Oeding, *The quadrfocal variety*, Linear Algebra and Its Applications **512** (2017), 306–330.
146. Magnus Oskarsson, Andrew Zisserman, and Kalle Åström, *Minimal projective reconstruction for combinations of points and lines in three views*, Image and Vision Computing **22** (2004), no. 10, 777–785.
147. Onur Özyeşil, Vladislav Voroninski, Ronen Basri, and Amit Singer, *A survey of structure from motion*, Acta Numerica **26** (2017), 305–364.
148. Sung-Il Pae and Jean Ponce, *On computing structural changes in evolving surfaces and their appearance*, International Journal of Computer Vision **43** (2001), no. 2, 113–131.

149. Tomas Pajdla, *Stereo with oblique cameras*, International Journal of Computer Vision **47** (2002), no. 1, 161–170.
150. Sylvain Petitjean, *The complexity and enumerative geometry of aspect graphs of smooth surfaces*, Algorithms in Algebraic Geometry and Applications, Springer, 1996, pp. 317–352.
151. Sylvain Petitjean, Jean Ponce, and David J Kriegman, *Computing exact aspect graphs of curved objects: Algebraic surfaces*, International Journal of Computer Vision **9** (1992), no. 3, 231–255.
152. Jean Ponce, *What is a camera?*, Proceedings of the IEEE Conference on Computer Vision and Pattern Recognition, 2009, pp. 1526–1533.
153. Jean Ponce and David J Kriegman, *Computing exact aspect graphs of curved objects: Parametric surfaces*, no. 1579, Department of Computer Science, University of Illinois at Urbana-Champaign, 1990.
154. Jean Ponce, Bernd Sturmfels, and Mathew Trager, *Congruences and concurrent lines in multi-view geometry*, Advances in Applied Mathematics **88** (2017), 62–91.
155. Andrew Pryhuber, Rainer Sinn, and Rekha Thomas, *Existence of two view chiral reconstructions*, SIAM Journal on Applied Algebra and Geometry **6** (2022), no. 1, 41–76.
156. Srikumar Ramalingam and Peter Sturm, *Minimal solutions for generic imaging models*, Proceedings of the IEEE Conference on Computer Vision and Pattern Recognition, 2008, pp. 1–8.
157. Kurt Reidemeister, *Knotentheorie*, Ergebnisse der Mathematik und ihrer Grenzgebiete, vol. 1, Springer-Verlag, 1932.
158. Fabio Remondino, Luigi Barazzetti, Francesco Nex, Marco Scaioni, and Daniele Sarazzi, *UAV photogrammetry for mapping and 3D modeling – Current status and future perspectives*, The International Archives of the Photogrammetry, Remote Sensing and Spatial Information Sciences **38** (2012), 25–31.
159. Joachim H Rieger, *Global bifurcation sets and stable projections of nonsingular algebraic surfaces*, International Journal of Computer Vision **7** (1992), no. 3, 171–194.
160. ———, *Computing view graphs of algebraic surfaces*, Journal of Symbolic Computation **16** (1993), no. 3, 259–272.
161. David M Rosen, Luca Carlone, Afonso S Bandeira, and John J Leonard, *SE-Sync: A certifiably correct algorithm for synchronization over the special Euclidean group*, The International Journal of Robotics Research **38** (2019), no. 2-3, 95–125.
162. George Salmon, *A treatise on the analytic geometry of three dimensions*, 4 ed., Dublin, 1882.
163. Olivier Saurer, Mare Pollefeys, and Gim Hee Lee, *A minimal solution to the rolling shutter pose estimation problem*, 2015 IEEE/RSJ International Conference on Intelligent Robots and Systems, 2015, pp. 1328–1334.
164. Johannes L Schonberger and Jan-Michael Frahm, *Structure-from-motion revisited*, Proceedings of the IEEE Conference on Computer Vision and Pattern Recognition, 2016, pp. 4104–4113.
165. Beniamino Segre, *Sulla caratterizzazione delle curve di diramazione dei piani multipli generali*, Memorie Della R. Accad. d’Italia **1** (1930), 5–31.
166. Andrew J Sommese and Charles W Wampler, *The numerical solution of systems of polynomials arising in engineering and science*, World Scientific, 2005.
167. Henrik Stewénus, David Nistér, Fredrik Kahl, and Frederik Schaffalitzky, *A minimal solution for relative pose with unknown focal length*, Image and Vision Computing **26** (2008), no. 7, 871–877.
168. Henrik Stewénus, Frederik Schaffalitzky, and David Nistér, *How hard is 3-view triangulation really?*, Proceedings of the IEEE International Conference on Computer Vision, 2005, pp. 686–693.
169. Peter Sturm, *Multi-view geometry for general camera models*, Proceedings of the IEEE Conference on Computer Vision and Pattern Recognition, 2005, pp. 206–212.
170. Rud Sturm, *Das problem der projectivität und seine anwendung auf die flächen zweiten grades*, Mathematische Annalen **1** (1869), no. 4, 533–574.
171. Bernd Sturmfels, *The Hurwitz form of a projective variety*, Journal of Symbolic Computation **79** (2017), 186–196.
172. Richard Szeliski, *Computer vision: Algorithms and applications*, Springer Science & Business Media, 2010.

173. SriRam Thirthala and Marc Pollefeys, *Radial multi-focal tensors*, International Journal of Computer Vision **96** (2012), no. 2, 195–211.
174. René Thom, *Structural stability and morphogenesis*, W.A. Benjamin, Inc., 1972.
175. Matthew Trager, Martial Hebert, and Jean Ponce, *The joint image handbook*, Proceedings of the IEEE International Conference on Computer Vision, 2015, pp. 909–917.
176. Matthew Trager, Brian Osserman, and Jean Ponce, *On the solvability of viewing graphs*, European Conference on Computer Vision, Springer, 2018, pp. 321–335.
177. Matthew Trager, Bernd Sturmfels, John Canny, Martial Hebert, and Jean Ponce, *General models for rational cameras and the case of two-slit projections*, Proceedings of the IEEE Conference on Computer Vision and Pattern Recognition, 2017, pp. 1935–1943.
178. Bill Triggs, *Matching constraints and the joint image*, Proceedings of the IEEE International Conference on Computer Vision, 1995, pp. 338–343.
179. Bill Triggs, Philip McLauchlan, Richard Hartley, and Andrew Fitzgibbon, *Bundle adjustment — a modern synthesis*, International Workshop on Vision Algorithms, Springer, 1999, pp. 298–372.
180. Manolis C Tsakiris and Rene Vidal, *Filtrated algebraic subspace clustering*, SIAM Journal on Imaging Sciences **10** (2017), no. 1, 372–415.
181. Jonathan Ventura, Clemens Arth, and Vincent Lepetit, *An efficient minimal solution for multi-camera motion*, Proceedings of the IEEE International Conference on Computer Vision, 2015, pp. 747–755.
182. René Vidal and Yi Ma, *A unified algebraic approach to 2-D and 3-D motion segmentation and estimation*, Journal of Mathematical Imaging and Vision **25** (2006), no. 3, 403–421.
183. René Vidal, Yi Ma, and Shankar Sastry, *Generalized principal component analysis (GPCA)*, IEEE Transactions on Pattern Analysis and Machine Intelligence **27** (2005), no. 12, 1945–1959.
184. René Vidal, Yi Ma, Stefano Soatto, and Shankar Sastry, *Two-view multibody structure from motion*, International Journal of Computer Vision **68** (2006), no. 1, 7–25.
185. Tomas Werner, *Combinatorial constraints on multiple projections of a set of points.*, Proceedings of IEEE International Conference on Computer Vision, 2003, pp. 1011–1016.
186. ———, *Constraint on five points in two images*, Proceedings of the IEEE Conference on Computer Vision and Pattern Recognition, vol. 2, 2003, pp. II–203.
187. Tomas Werner and Tomas Pajdla, *Cheirality in epipolar geometry*, Proceedings of IEEE International Conference on Computer Vision, vol. 1, 2001, pp. 548–553.
188. ———, *Oriented matching constraints.*, British Machine Vision Conference, 2001, pp. 1–10.
189. Lior Wolf and Amnon Shashua, *On projection matrices $\mathbb{P}^k \rightarrow \mathbb{P}^2, k = 3, \dots, 6$, and their applications in computer vision*, International Journal of Computer Vision **48** (2002), no. 1, 53–67.
190. Heng Yang and Luca Carlone, *Certifiably optimal outlier-robust geometric perception: Semi-definite relaxations and scalable global optimization*, IEEE Transactions on Pattern Analysis and Machine Intelligence **45** (2022), no. 3, 2816–2834.
191. Oscar Zariski, *On the problem of existence of algebraic functions of two variables possessing a given branch curve*, American Journal of Mathematics **51** (1929), no. 2, 305–328.
192. Ji Zhao, Laurent Kneip, Yijia He, and Jiayi Ma, *Minimal case relative pose computation using ray-point-ray features*, IEEE Transactions on Pattern Analysis and Machine Intelligence **42** (2019), no. 5, 1176–1190.
193. Ming Zhao and Ronald Chung, *Critical configurations of lines to geometry determination of three cameras*, 19th International Conference on Pattern Recognition, IEEE, 2008, pp. 1–5.

DEPARTMENT OF MATHEMATICS AND ODEN INSTITUTE, UNIVERSITY OF TEXAS AT AUSTIN
 Email address: jkileel@math.utexas.edu

INSTITUTIONEN FÖR MATEMATIK, KTH ROYAL INSTITUTE OF TECHNOLOGY
 Email address: kathlen@kth.se